remote sensing

MDPI

Article

Evaluation of MODIS Gross Primary Production across Multiple Biomes in China Using Eddy Covariance Flux Data

Hongji Zhu [1,†], Aiwen Lin [1,*], Lunche Wang [2,*,†], Yu Xia [1] and Ling Zou [1]

1 School of Resource and Environmental Science, Wuhan University, Wuhan 430079, China; zhuhongji@whu.edu.cn (H.Z.); xysw@whu.edu.cn (Y.X.); cheryl_zou@whu.edu.cn (L.Z.)

2 Laboratory of Critical Zone Evolution, School of Earth Sciences, China University of Geosciences, Wuhan 430074, China

* Correspondence: awlin@whu.edu.cn (A.L.); wang@cug.edu.cn (L.W.); Tel.: +86-137-0719-1591 (A.L.); +86-133-4988-9828 (L.W.)

† These authors contributed equally to this work.

Academic Editors: Richard L. Miller, Cheng-Chien Liu, Clement Atzberger and Prasad S. Thenkabail

Received: 22 March 2016; Accepted: 2 May 2016; Published: 13 May 2016

Abstract: MOD17A2 provides near real-time estimates of gross primary production (GPP) globally. In this study, MOD17A2 GPP was evaluated using eddy covariance (EC) flux measurements at eight sites in five various biome types across China. The sensitivity of MOD17A2 to meteorological data and leaf area index/fractional photosynthetically active radiation (LAI/FPAR) products were examined by introducing site meteorological measurements and improved Global Land Surface Satellite (GLASS) LAI products. We also assessed the potential error contributions from land cover and maximum light use efficiency (ε_{max}). The results showed that MOD17A2 agreed well with flux measurements of annual GPP (R^2 = 0.76) when all biome types were considered as a whole. However, MOD17A2 was ineffective for estimating annual GPP at mixed forests, evergreen needleleaf forests and croplands, respectively. Moreover, MOD17A2 underestimated flux derived GPP during the summer (R^2 = 0.46). It was found that the meteorological data used in MOD17A2 failed to properly estimate the site measured vapor pressure deficits (VPD) (R^2 = 0.31). Replacing the existing LAI/FPAR data with GLASS LAI products reduced MOD17A2 GPP uncertainties. Though land cover presented the fewest errors, ε_{max} prescribed in MOD17A2 were much lower than inferred ε_{max} calculated from flux data. Thus, the qualities of meteorological data and LAI/FPAR products need to be improved, and ε_{max} should be adjusted to provide better GPP estimates using MOD17A2 for Chinese ecosystems.

Keywords: MODIS; gross primary production (GPP); validation; eddy covariance; China

1. Introduction

Gross primary production (GPP), which is defined as the overall photosynthetic fixation of carbon by plants, is an important variable in studies of the carbon balance between the atmosphere and biosphere [1,2]. GPP is also the basis for essential ecosystem services such as food, fiber, fuel and construction materials [3]. Thus, the quantification of GPP has become a topic of wide concern in global change studies [4–7].

By using optical and near-infrared spectral wavelengths, GPP can be estimated from satellite remote sensing [8,9]. In particular, the Moderate Resolution Imaging Spectroradiometer (MODIS) primary production products (MOD17A2) are the first regular, near-real-time GPP datasets for the repeated monitoring of global vegetation at a 1-km resolution every eight days [10]. Zhao *et al.* (2005) [11] had demonstrated that MODIS GPP fitted well with GPP derived from 12 flux towers over

North America, indicating MOD17A2 were reliable products. However, for MODIS GPP products, there are still exist many potential sources of errors that arise from the input datasets, the parameters used to describe the biophysical behavior of vegetation, and the algorithm itself [12]. First, there is a large disparity between the spatial resolution of meteorological data and the resolution of MODIS products, which will provide inaccurate atmospheric conditions at scales consistent with land surface heterogeneities [13]. Second, the MODIS leaf area index (LAI) has a poor correlation with the ground measurements, which will lead to an erroneous estimation for fraction of photosynthetically active radiation (FPAR) [11]. Third, the accuracy of MODIS land cover classification is not very satisfactory, and most mistakes are between similar classes [14]. Finally, it does not conform to reality to assign a constant value of maximum light use efficiency (LUE) to the same biome type [5]. As a result, each of these error sources (*i.e.*, meteorology, LAI/FPAR, land cover and LUE) requires a corresponding validation procedure and must be examined separately [15].

The error analysis of MODIS GPP products is a challenging task because of the difficulty in making direct measurements of GPP values. One widely used approach uses the eddy covariance (EC) technique, which measures the fluxes of carbon, water and energy between the atmosphere and land [16,17]. A number of validation efforts have been established to evaluate the accuracy of MOD17A2 products that use time series comparisons between MODIS-based and EC flux tower-based GPP for one or more 1-km^2 cells centered on towers [18,19]. Turner *et al.* (2003) [20] evaluated the MODIS GPP products at two sites: a temperate forest site and a boreal forest site. Their results showed that, relative to the flux tower measurements, MODIS overestimated the GPP by 35% at the boreal forest site, but the MODIS estimates were comparable to the tower results for the temperate forest site. Heinsch *et al.* (2006) [14] carried out a comprehensive evaluation of MOD17A2 by comparing MODIS-based GPP to flux tower-based GPP at 15 research sites in six different biome classes across North America. The authors reported that the MODIS GPP products overestimated the tower-based calculations by 20%–30% on average. They further found that the use of MODIS GPP products with DAO (NASA'S Data Assimilation Office) meteorology overestimated the annual GPP, whereas the use of tower-specific meteorology in the MODIS GPP calculations led to underestimates. The performance of MODIS GPP in Africa has also been evaluated using *in situ* measurements of meteorology and flux tower GPP for 12 sites. The study indicated that MOD17A2 agreed well with the tower-based GPP for wet sites, whereas the estimates were too small for dry sites [21].

Based on EC flux data provided by the Chinese FLUX Observation and Research Network (ChinaFLUX), several studies have assessed the performances of MODIS GPP in Chinese different biome types [22,23]. For example, Zhang *et al.* (2008) [24] evaluated MODIS GPP by using estimated GPP from EC flux measurements over an alpine meadow on the Tibetan Plateau. Their results showed that the mean annual MODIS GPP accounted for 1/2–2/3 of the flux-based GPP in the study region. Liu *et al.* (2015) [25] reported that MODIS GPP performed poorly for evergreen forests but provided accurate estimates for grassland and mixed forests. However, these studies explored error sources mainly focused on one or two aspects, while comprehensive and detailed error analyses are still needed. Thus, we not only methodically evaluated the eight-day, seasonal and annual MODIS GPP against tower GPP, but also carefully analyzed each input. In this paper, we evaluated MOD17A2 GPP using EC flux tower data at eight sites in five various biome types across China (Figure 1 and Table 1). The objectives of our study were to evaluate the performance of MOD17A2 in China through comparisons with GPP measured at EC flux towers and to examine the potential error contributions of all input variables (meteorology, LAI/FPAR, land cover and LUE) used in the algorithm.

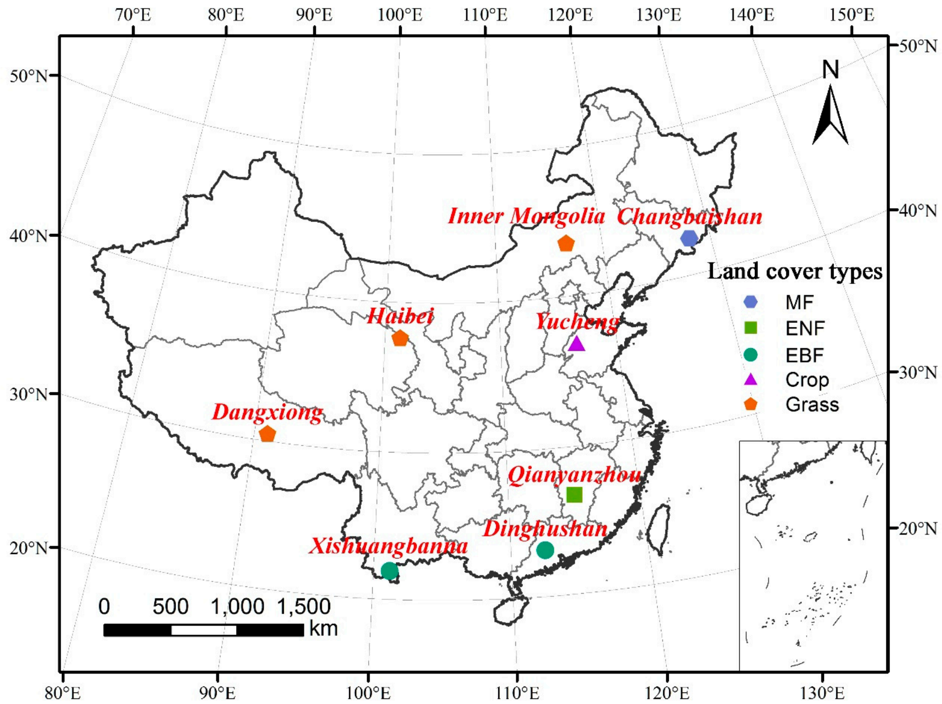

Figure 1. Locations of the eight flux tower sites used in this study. MF: Mixed forest; ENF: Evergreen needleleaf forests; EBF: Evergreen broadleaf forests; Crop: Croplands; Grass: Grasslands.

Table 1. Site descriptions including name (abbreviation), latitude and longitude (lat/long, decimal degrees), general biome type, mean annual long-term precipitation (MAP, mm), mean annual temperature (MAT, °C), years of measurements and references. MF: Mixed forest; ENF: Evergreen needleleaf forests; EBF: Evergreen broadleaf forests; Crop: Croplands; Grass: Grasslands.

Sites (Abbreviation)	Lat (°N)	Lon (°E)	Biome Type	MAP (mm)	MAT (°C)	Data Range	References
Changbaishan forest site (CBS)	42.40	128.10	MF	713	3.6	2003–2005	Guan *et al.* (2006) [26]
Qianyanzhou forest site (QYZ)	26.74	115.06	ENF	1542	17.9	2003–2005	Wen *et al.* (2006) [27]
Dinghushan forest site (DHS)	23.17	112.53	EBF	1956	20.9	2003–2005	Zhang *et al.* (2006) [28]
Xishuangbanna forest site (XSBN)	21.95	101.20	EBF	1493	21.8	2003–2005	Yu *et al.* (2006) [29]
Yucheng cropland site (YC)	36.83	116.57	Crop	582	13.1	2003–2005	Sun *et al.* (2006) [30]
Haibei grassland site (HB)	37.67	101.33	Grass	580	−1.7	2003–2005	Fu *et al.* (2006) [31]
Inner Mongolia grassland site (NMG)	43.55	116.68	Grass	338	0.9	2004–2005	Fu *et al.* (2006) [31]
Dangxiong grassland site (DX)	30.50	91.07	Grass	450	1.3	2004–2005	Yu *et al.* (2006) [29]

2. Materials and Methods

2.1. Materials

2.1.1. MODIS GPP Algorithm

The GPP calculation used in the MODIS GPP algorithm (MOD17A2) is based on the original logic of Monteith (1972) [32] that relates gross photosynthesis to the amount of photosynthetically active radiation (PAR) absorbed by plants over a growing season. As described in detail by Running *et al.* (2000) [33], the algorithm was developed as follows:

$$\text{GPP} = \text{PAR} \times \text{FPAR} \times \varepsilon \tag{1}$$

where FPAR is the fraction of PAR absorbed by the vegetation canopy, and PAR is determined as a fraction of the downward solar shortwave radiation (SWRad):

$$\text{PAR} = \text{SWRad} \times 0.45 \tag{2}$$

The magnitude of LUE ε in Equation (1) is calculated as

$$\varepsilon = \varepsilon_{\text{max}} \times \text{T}_\text{s} \times \text{VPD}_\text{s} \tag{3}$$

where ε_{max} is the maximum LUE obtained from a Biome Properties Look-Up Table (BPLUT) on the basis of biome type, and T_s and VPD_s are the attenuation scalars from cold temperature (low daily minimum temperature, T_{min}) and water stresses (high daily vapor pressure deficit, VPD), respectively [34,35].

Following the MODIS GPP algorithm, essential MODIS product images from 2003 to 2005 were downloaded from the Level 1 and Atmosphere Archive and Distribution System (LAADS) website [36]. Using the latitudes and longitudes of the flux tower sites, we obtained 5 km × 5 km cutouts centered over each tower location that represented the: (1) land cover classification (MCD12Q1, C5.1, 500-m resolution, annual product); (2) LAI and FPAR (MOD15A2, C5, 1-km resolution, eight-day product); and (3) GPP (MOD17A2, C5.5, 1-km resolution, eight-day product).

In particular, MCD12Q1 is used in the MOD15A2 and MOD17A2 calculations. Unlike the MOD15A2 algorithm, which uses MCD12Q1 Land Cover Classification Type 3 (LAI/FPAR scheme) to calculate FPAR, the MOD17A2 algorithm uses MCD12Q1 Land Cover Classification Type 2 (University of Maryland land cover classification scheme) to map biome-specific physiological parameters (ε_{max}, maximum and minimum air temperature and VPD) according to the BPLUT [37].

2.1.2. Meteorological Data

- NCEP-DOE Reanalysis II Data

The MODIS GPP Collection 5.5 (MOD17A2, C5.5) data used in this paper implement National Center for Environmental Prediction-Department of Energy (NCEP-DOE) Reanalysis II data for direct meteorological inputs. For each flux tower site, six-hour data composed of air temperature (T_{air}, °C), downward shortwave radiation (SWRad, $W \cdot m^{-2}$), surface pressure (Pres, Pa), and specific humidity (SH, $kg \cdot kg^{-1}$) for 2003–2005 were downloaded from the Earth System Research Laboratory (ESRL) [38]. From these data, we obtained the daily average air temperature (T_{avg}, °C), daily minimum air temperature (T_{min}, °C), daily average VPD (VPD_{avg}, Pa), and daily total SWRad ($MJ \cdot m^{-2} \cdot d^{-1}$) at a 1.9° × 1.9° resolution. To interpolate the 1.9° × 1.9° resolution NCEP-DOE data down to the 1-km MODIS pixel resolution, the daily data for each pixel were interpolated using a spatial nonlinear interpolation scheme following Zhao *et al.* (2005) [11].

- Site Meteorological Data

Site meteorological data (PAR, air temperature and VPD) during 2003–2005 were obtained directly from the flux towers or were derived from meteorological station data provided by the China Meteorological Administration (CMA) [39]. Based on the half-hourly flux tower measurements, which are composed of air temperature (T_{air}, °C) and either PAR (μmol· m^{-2}· s^{-1}) or downward shortwave radiation (SWRad, W· m^{-2}), we obtained the daily T_{avg}, T_{min} and PAR. In addition, the daily average e_a (*i.e.*, the actual air vapor pressure, Pa) and daily average RH (*i.e.*, relative humidity, %) were selected from the meteorological station datasets to calculate VPD_{avg} [40]. The site meteorological data (T_{avg}, T_{min}, PAR and VPD_{avg}) were then directly compared to the NCEP-DOE Reanalysis II data to evaluate how well the reanalysis datasets represented the local climatic conditions.

2.1.3. GLASS LAI Data

For the MODIS GPP algorithm, the FPAR is an essential input. To examine the potential error contributions from LAI/FPAR, the Global Land Surface Satellite Leaf Area Index (GLASS LAI) products, which are an improved LAI dataset, were introduced into our study [41]. The GLASS LAI algorithm uses general regression neural networks (GRNNs) to retrieve LAI data. In addition, the GRNNs are trained by the fused LAI values from time-series multi-sensor remote sensing data, including MODIS and CYCLOPES LAI products and the corresponding reprocessed MODIS reflectance values [42]. It has been demonstrated that the GLASS LAI algorithm is able to produce temporally continuous LAI datasets with significantly improved accuracies compared with current MODIS and CYCLOPES LAI products [43]. In this paper, the GLASS LAI subsets (0.05° × 0.05° resolution, eight-day interval) during the 2003 to 2005 period centered over each of the flux tower locations were obtained from the Generation and Applications of Global Products of Essential Land Variables website [44].

Using a simple Beer's Law approach [45], the GLASS LAI data can be converted to FPAR data by:

$$\text{FPAR} = 1 - e^{(-K) \times \text{LAI}} \tag{4}$$

where K is the canopy light extinction coefficient, which is set to 0.5. To explore the influence of FPAR on GPP, we replaced the MOD15A2 FPAR with the above FPAR, which originated from GLASS LAI, to recalculate MODIS GPP in this study.

2.1.4. EC Flux Data

Eight EC flux tower sites across China were included in this study (Figure 1). The sites cover a diversity of biome types and climate regimes, including mixed forests, evergreen needleleaf forests, evergreen broadleaf forests, croplands and grasslands [29]. A brief description of the sites is presented in Table 1, and detailed information is available at the ChinaFLUX website [46].

The EC flux data measured at the eight flux tower sites for 2003–2005 were downloaded from the ChinaFLUX website. The daily values, which were composed of the net ecosystem exchange (NEE) and ecosystem respiration (Re), were used to calculate GPP:

$$\text{GPP} = \text{Re} - \text{NEE} \tag{5}$$

where the GPP values are in units of gC· m^{-2}· d^{-1} [47]. For consistency with the time interval of the MODIS GPP products, we then aggregated eight-day flux derived GPP from the calculated daily values.

2.2. Methods

2.2.1. Experimental Design

To differentiate the effects of the meteorological elements and LAI/FPAR on the GPP estimates, we designed the following four experimental groups to recalculate GPP under different scenarios. (1) Following the standard MOD17A2 products completely, NCEP-DOE Reanalysis II meteorology data and MOD15A2 LAI/FPAR products were used to estimate GPP (MOD_NCEP GPP); (2) Site meteorology data and MOD15A2 LAI/FPAR products were used to estimate GPP (MOD_Tower GPP); (3) NCEP-DOE meteorology data and GLASS LAI/FPAR products were used to estimate GPP (NCEP_GLASS GPP); (4) Site meteorology data and GLASS LAI/FPAR products were used to estimate GPP (Tower_GLASS GPP). Finally, all the GPP estimates were directly compared with the EC flux derived GPP (Flux_Tower GPP) to assess their accuracies and uncertainties.

2.2.2. Analytical Methods

In this study, the computation results for eight-day, seasonal and annual GPP had been analyzed, respectively. We firstly calculated the daily GPP, and then integrated the daily GPP into eight-day, seasonal and annual GPP by accumulating. The sensitivity of MOD17A2 algorithm to meteorological data and LAI/FPAR products were examined by introducing site meteorological measurements and improved GLASS LAI products. We also assessed the potential error contributions from land cover and ε_{max}. Four statistic indices were used to evaluate the accuracies and uncertainties: (1) the coefficient of determination (R^2), which represents the amount of variation in the observations explained by the simulations; (2) bias, which quantifies the difference between the simulations and the observations; (3) the root mean square error (RMSE, %), which is computed as

$$\mathrm{RMSE}\ (\%) = \frac{1}{\overline{\mathrm{O}}} \times \sqrt{\frac{1}{n} \times \sum_{i=1}^{n} (\mathrm{S_i} - \mathrm{O_i}^2)} \times 100 \tag{6}$$

where $\overline{\mathrm{O}}$ is the average value of the observed data, and S_i and O_i are the simulated and observed values, respectively; and Equation (4) the relative error (RE, %), which is

$$\mathrm{RE}\ (\%) = \frac{1}{n} \times \sum_{i=1}^{n} \left(\frac{\mathrm{S_i} - \mathrm{O_i}}{\mathrm{O_i}}\right) \times 100 \tag{7}$$

3. Results

3.1. GPP Validation

3.1.1. Eight-Day GPP

The tower-based GPP measurements (Flux_Tower GPP) were compared with the results of the four experimental groups (*i.e.*, MOD_NCEP GPP, MOD_Tower GPP, NCEP_GLASS GPP, and Tower_GLASS GPP) over eight days (Figure 2). Overall, when compared with the MOD_NCEP GPP algorithm (R^2 = 0.55), the remaining three algorithms, particularly the NCEP_GLASS GPP (R^2 = 0.65) and Tower_GLASS GPP (R^2 = 0.66) algorithms, were more effective at estimating the Flux_Tower GPP.

From the perspective of a single site, in CBS, QYZ and YC, all four algorithms (MOD_NCEP GPP, MOD_Tower GPP, NCEP_GLASS GPP, and Tower_GLASS GPP) underestimated the Flux_Tower GPP to varying degrees (Figure 3, Table 2). The MOD_Tower GPP were the most underestimated (-13 gC·m^{-2}·8-day^{-1} for CBS, -18 gC·m^{-2}·8-day^{-1} for QYZ and -22 gC·m^{-2}·8-day^{-1} for YC), and the NCEP_GLASS GPP were the least underestimated (-1 gC·m^{-2}·8-day^{-1} for CBS, -2 gC·m^{-2}·8-day^{-1} for QYZ and -14 gC·m^{-2}·8-day^{-1} for YC). However, for NMG, all four algorithms overestimated the Flux_Tower GPP. The MOD_NCEP GPP were the most overestimated

(3 gC· m^{-2}· 8-day^{-1}), and the NCEP_GLASS GPP and Tower_GLASS GPP were the least overestimated (1 gC· m^{-2}· 8-day^{-1}). For the other sites, some algorithms overestimated the Flux_Tower GPP, whereas some underestimated them. For CBS, QYZ and DHS, the Tower_GLASS GPP algorithm most effectively estimated the Flux_Tower GPP (R^2 = 0.92, R^2 = 0.87 and R^2 = 0.75, respectively), and the greatest improvements were obtained over the MOD_NCEP GPP algorithm (R^2 = 0.76, R^2 = 0.52 and R^2 = 0.30) in particular. However, for YC and NMG, the Tower_GLASS GPP algorithm was not as effective as the other three algorithms for estimating the Flux_Tower GPP. In the case of YC, the performance of the Tower_GLASS GPP algorithm (R^2 = 0.77) was close to that of the most effective algorithm (MOD_NCEP GPP, R^2 = 0.81). However, for NMG, the gap between the Tower_GLASS GPP (R^2 = 0.64) and the best estimating algorithm (MOD_Tower GPP, R^2 = 0.75) was large. For HB and DX, all four algorithms effectively estimated the Flux_Tower GPP. In particular, the MOD_NCEP GPP (R^2 = 0.95, Bias = 0 gC· m^{-2}· 8-day^{-1}) and MOD_Tower GPP (R^2 = 0.89, Bias = 0 gC· m^{-2}· 8-day^{-1}) algorithms performed best for HB and DX, respectively. Regarding XSBN, however, no algorithm succeeded in estimating the Flux_Tower GPP.

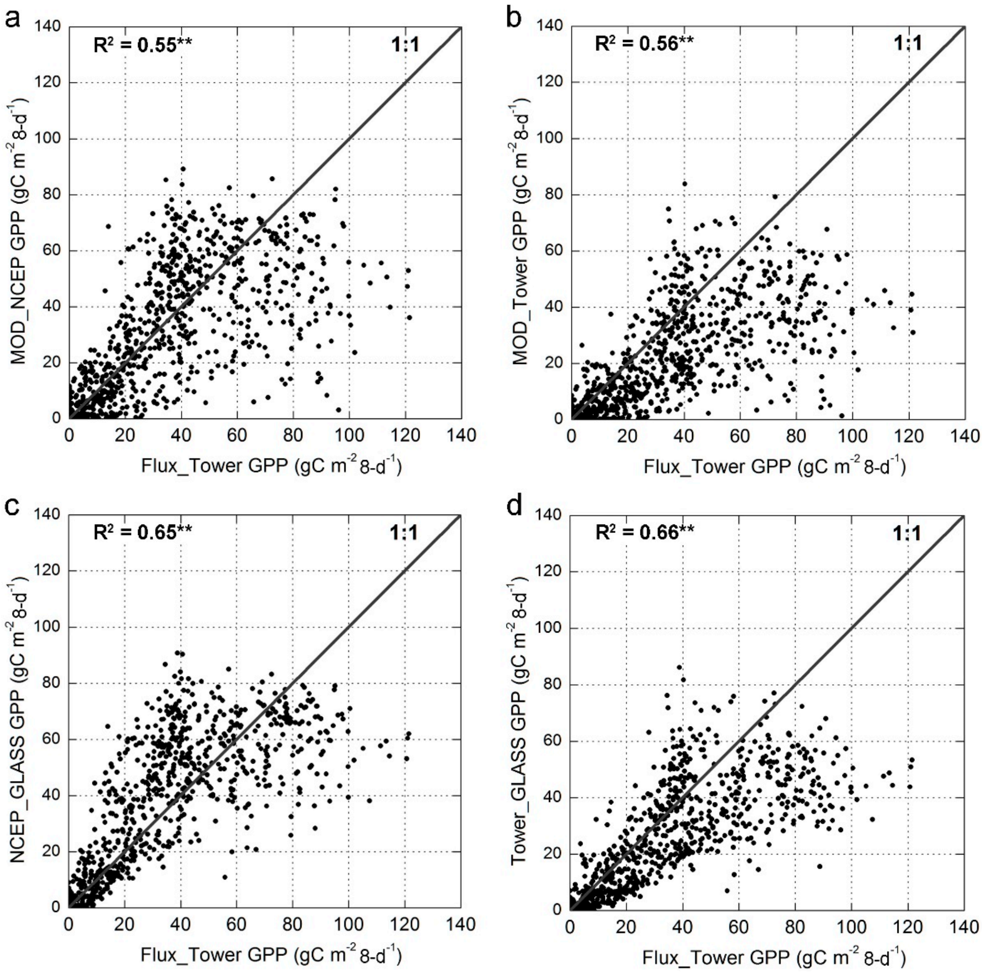

Figure 2. (**a**) Scatter plots of the eight-day MOD_NCEP GPP *vs.* the Flux_Tower GPP; (**b**) MOD_Tower GPP *vs.* the Flux_Tower GPP; (**c**) NCEP_GLASS GPP *vs.* the Flux_Tower GPP; and (**d**) Tower_GLASS GPP *vs.* the Flux_Tower GPP. Significance levels: ** $p < 0.01$.

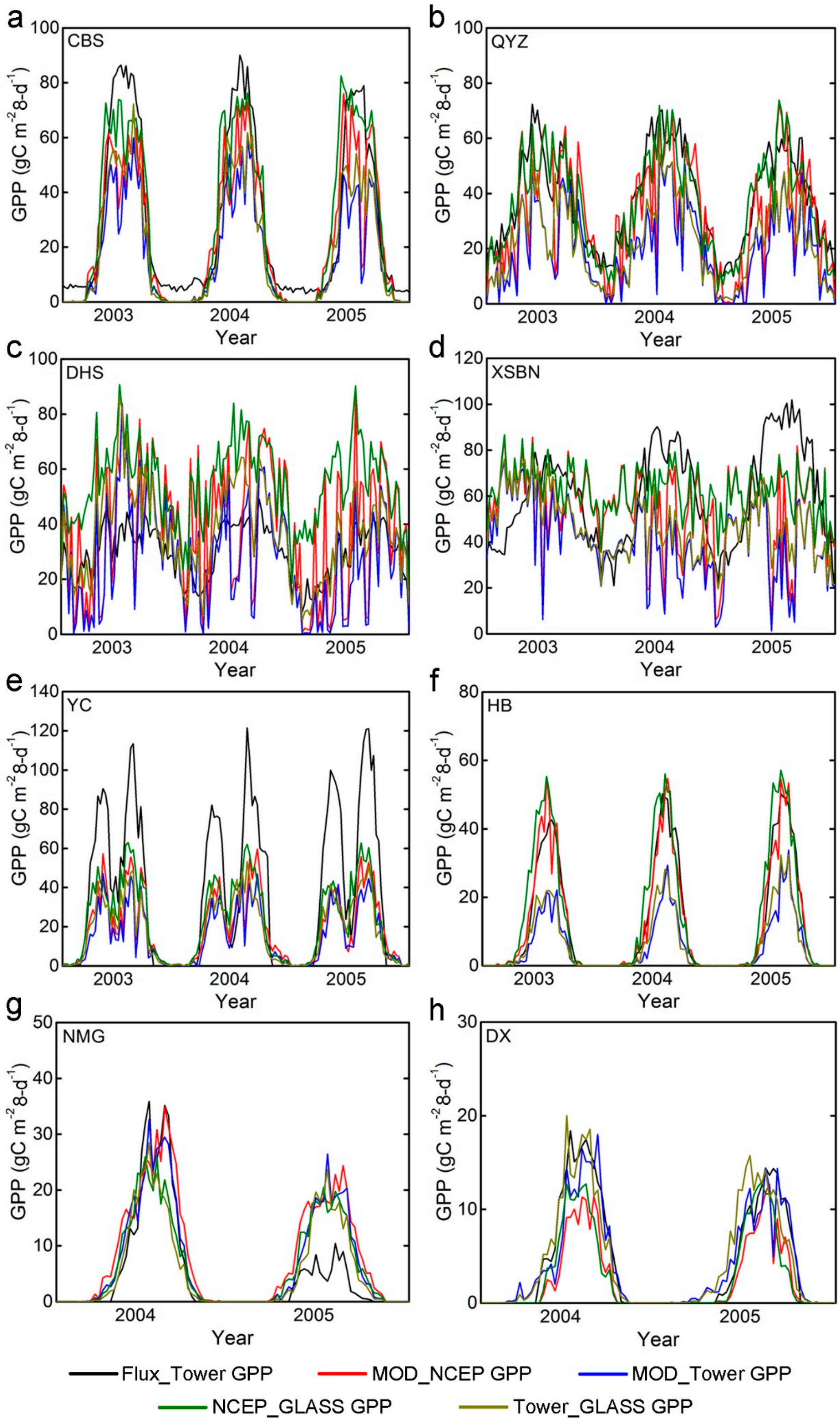

Figure 3. Time series of eight-day GPP derived from the tower estimates (*i.e.*, Flux_Tower GPP) and four different experimental groups (*i.e.*, MOD_NCEP GPP, MOD_Tower GPP, NCEP_GLASS GPP and Tower_GLASS GPP) at: (**a**) CBS forest site; (**b**) QYZ forest site; (**c**) DHS forest site; (**d**) XSBN forest site; (**e**) YC cropland site; (**f**) HB grassland site; (**g**) NMG grassland site; and (**h**) DX grassland site. The full name for each site is listed in Table 1.

Table 2. Comparison of eight-day GPP derived from the tower estimates with those derived from the MODIS algorithms (MOD_NCEP GPP, MOD_Tower GPP, NCEP_GLASS GPP, and Tower_GLASS GPP) at eight sites. The full name for each site is listed in Table 1.

Site	Comparison	R^2	Mean (SD) ($gC\cdot m^{-2}\cdot 8\text{-day}^{-1}$)	Bias ($gC\cdot m^{-2}\cdot 8\text{-day}^{-1}$)	RMSE (%)	RE (%)
CBS	Flux_Tower *vs.* MOD_NCEP	0.76 **	29(30) *vs.* 24(25)	−5	54	60
	Flux_Tower *vs.* MOD_Tower	0.83 **	29(30) *vs.* 16(19)	−13	68	59
	Flux_Tower *vs.* NCEP_GLASS	0.84 **	29(30) *vs.* 28(30)	−1	42	62
	Flux_Tower *vs.* Tower_GLASS	0.92 **	29(30) *vs.* 19(22)	−10	50	58
QYZ	Flux_Tower *vs.* MOD_NCEP	0.52 **	38(18) *vs.* 32(20)	−6	41	34
	Flux_Tower *vs.* MOD_Tower	0.66 **	38(18) *vs.* 20(15)	−18	55	54
	Flux_Tower *vs.* NCEP_GLASS	0.81 **	38(18) *vs.* 36(18)	−2	22	18
	Flux_Tower *vs.* Tower_GLASS	0.87 **	38(18) *vs.* 22(15)	−16	45	48
DHS	Flux_Tower *vs.* MOD_NCEP	0.30 **	30(10) *vs.* 38(24)	8	73	68
	Flux_Tower *vs.* MOD_Tower	0.42 **	30(10) *vs.* 27(19)	−3	51	45
	Flux_Tower *vs.* NCEP_GLASS	0.55 **	30(10) *vs.* 55(15)	25	90	95
	Flux_Tower *vs.* Tower_GLASS	0.75 **	30(10) *vs.* 36(17)	6	39	27
XSBN	Flux_Tower *vs.* MOD_NCEP	-	60(21) *vs.* 54(18)	−6	49	41
	Flux_Tower *vs.* MOD_Tower	-	60(21) *vs.* 41(17)	−19	55	38
	Flux_Tower *vs.* NCEP_GLASS	0.10 **	60(21) *vs.* 62(11)	2	34	35
	Flux_Tower *vs.* Tower_GLASS	0.07 **	60(21) *vs.* 46(13)	−14	43	31
YC	Flux_Tower *vs.* MOD_NCEP	0.81 **	37(39) *vs.* 19(18)	−18	80	-
	Flux_Tower *vs.* MOD_Tower	0.80 **	37(39) *vs.* 15(15)	−22	93	-
	Flux_Tower *vs.* NCEP_GLASS	0.79 **	37(39) *vs.* 23(20)	−14	72	-
	Flux_Tower *vs.* Tower_GLASS	0.77 **	37(39) *vs.* 21(19)	−16	78	-
HB	Flux_Tower *vs.* MOD_NCEP	0.95 **	12(16) *vs.* 12(17)	0	31	-
	Flux_Tower *vs.* MOD_Tower	0.94 **	12(16) *vs.* 5(8)	−7	92	-
	Flux_Tower *vs.* NCEP_GLASS	0.91 **	12(16) *vs.* 14(19)	2	52	-
	Flux_Tower *vs.* Tower_GLASS	0.94 **	12(16) *vs.* 6(9)	−6	84	-
NMG	Flux_Tower *vs.* MOD_NCEP	0.73 **	5(9) *vs.* 8(10)	3	124	-
	Flux_Tower *vs.* MOD_Tower	0.75 **	5(9) *vs.* 7(9)	2	106	-
	Flux_Tower *vs.* NCEP_GLASS	0.65 **	5(9) *vs.* 6(8)	1	112	-
	Flux_Tower *vs.* Tower_GLASS	0.64 **	5(9) *vs.* 6(8)	1	110	-
DX	Flux_Tower *vs.* MOD_NCEP	0.89 **	4(6) *vs.* 2(4)	−2	74	-
	Flux_Tower *vs.* MOD_Tower	0.89 **	4(6) *vs.* 4(5)	0	46	-
	Flux_Tower *vs.* NCEP_GLASS	0.86 **	4(6) *vs.* 3(4)	−1	65	-
	Flux_Tower *vs.* Tower_GLASS	0.88 **	4(6) *vs.* 5(6)	1	48	-

Significance levels: ** $p < 0.01$.

3.1.2. Seasonal GPP

The tower-based GPP measurements (Flux_Tower GPP) were compared with the results achieved by the four algorithms (*i.e.*, MOD_NCEP GPP, MOD_Tower GPP, NCEP_GLASS GPP, and Tower_GLASS GPP) over each season (Figures 4–7 and Table 3). Overall, the four algorithms effectively estimated the Flux_Tower GPP in the spring, autumn and winter. In particular, the algorithms had the best estimating effectiveness for the winter (the values of R^2 ranged from 0.87 to 0.92). However, the overall estimating effectiveness of the four algorithms was poor for the summer (values of R^2 ranged from 0.36 to 0.52). The details are as follows:

(1) Spring (March–May): The estimation performances of MOD_NCEP GPP (R^2 = 0.64) and Tower_GLASS GPP (R^2 = 0.65) were excellent (Figure 4, Table 3). The MOD_NCEP GPP, MOD_Tower GPP and Tower_GLASS GPP underestimated the Flux_Tower GPP to varying degrees (−39 $gC\cdot m^{-2}\cdot 3\text{-month}^{-1}$, −122 $gC\cdot m^{-2}\cdot 3\text{-month}^{-1}$ and −80 $gC\cdot m^{-2}\cdot 3\text{-month}^{-1}$, respectively), primarily because of the considerable underestimation for QYZ and YC (Figure 4a,b,d). In contrast, NCEP_GLASS GPP overestimated the Flux_Tower GPP (40 $gC\cdot m^{-2}\cdot 3\text{-month}^{-1}$) because the measurements for DHS were considerably overestimated (Figure 4c).

(2) Summer (June–August): None of the four algorithms estimated the Flux_Tower GPP effectively (Figure 5, Table 3). The main reason that the Flux_Tower GPP were seriously

underestimated by the MOD_NCEP GPP, MOD_Tower GPP and Tower_GLASS GPP algorithms (-143 gC· m^{-2}· 3-month^{-1}, -254 gC· m^{-2}· 3-month^{-1} and -161 gC· m^{-2}· 3-month^{-1}, respectively) was that the measurements for CBS, QYZ, XSBN and YC were considerably underestimated (Figure 5a,b,d).

(3) Autumn (September–November): The MOD_NCEP GPP (R^2 = 0.80, Bias = 0 gC· m^{-2}· 3-month^{-1} and RMSE = 32%) and NCEP_GLASS GPP (R^2 = 0.76, Bias = 1 gC· m^{-2}· 3-month^{-1} and RE = 57%) provided better estimating effectiveness (Figure 6, Table 3). In contrast, the MOD_Tower GPP and Tower_GLASS GPP obviously underestimated the Flux_Tower GPP (-102 gC· m^{-2}· 3-month^{-1}) as a result of the common underestimations for CBS, HB, QYZ, XSBN and YC (Figure 6b,d).

(4) Winter (January–February and December): All four algorithms effectively estimated the Flux_Tower GPP (Figure 7, Table 3). However, the MOD_NCEP GPP and NCEP_GLASS GPP algorithms seriously overestimated the Flux_Tower GPP for DHS and XSBN (Figure 7a,c). The Flux_Tower GPP for QYZ were severely underestimated by the MOD_Tower GPP and Tower_GLASS GPP algorithms (Figure 7b,d).

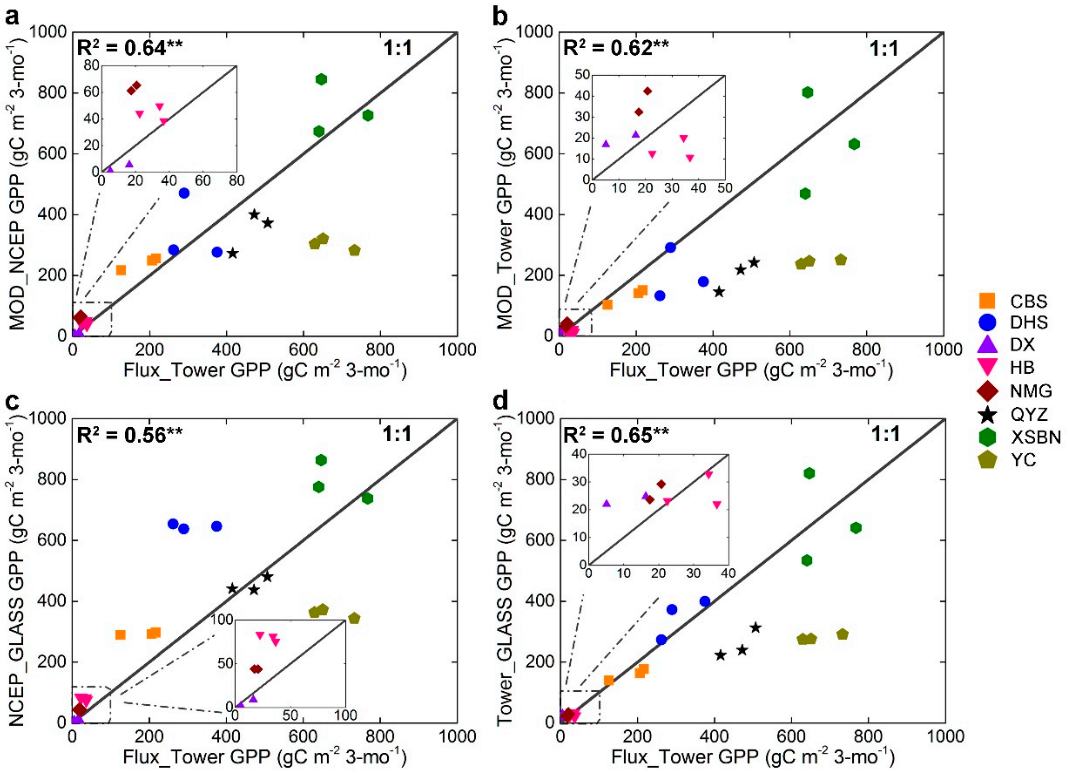

Figure 4. Comparisons of Flux_Tower GPP for spring (March–May) with: (**a**) MOD_NCEP GPP; (**b**) MOD_Tower GPP; (**c**) NCEP_GLASS GPP; and (**d**) Tower_GLASS GPP. Significance levels: ** $p < 0.01$.

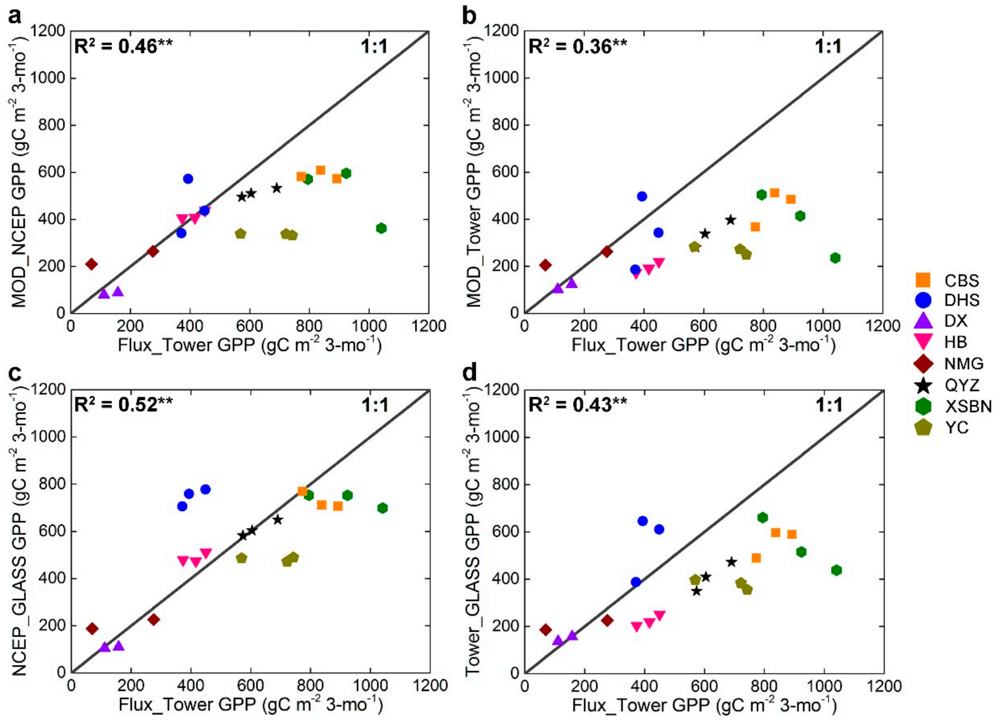

Figure 5. Comparisons of Flux_Tower GPP for summer (June–August) with: (**a**) MOD_NCEP GPP; (**b**) MOD_Tower GPP; (**c**) NCEP_GLASS GPP; and (**d**) Tower_GLASS GPP. Significance levels: ** $p < 0.01$.

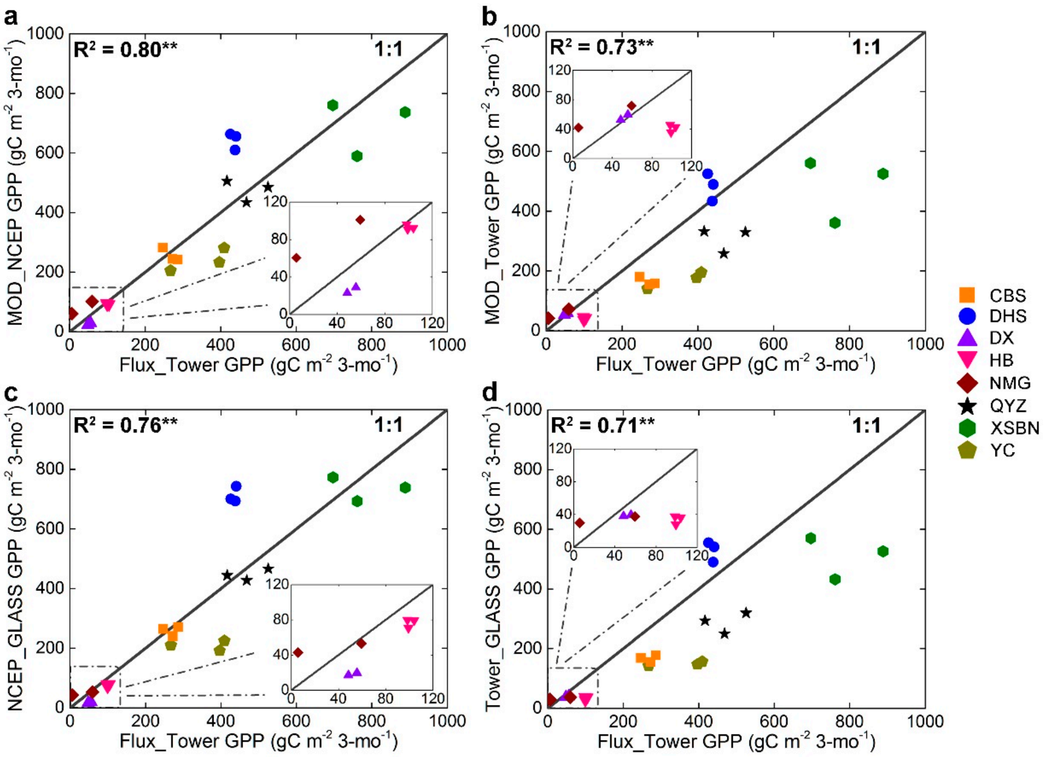

Figure 6. Comparisons of Flux_Tower GPP for autumn (September–November) with: (**a**) MOD_NCEP GPP; (**b**) MOD_Tower GPP; (**c**) NCEP_GLASS GPP; and (**d**) Tower_GLASS GPP. Significance levels: ** $p < 0.01$.

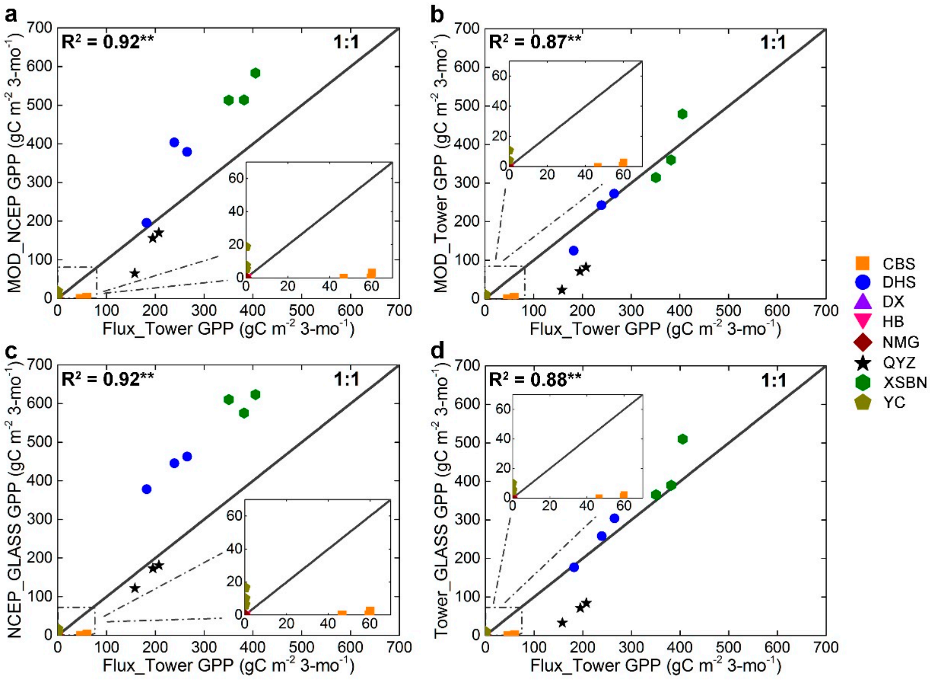

Figure 7. Comparisons of Flux_Tower GPP for winter (January, February and December) with: (**a**) MOD_NCEP GPP; (**b**) MOD_Tower GPP; (**c**) NCEP_GLASS GPP; and (**d**) Tower_GLASS GPP. Significance levels: ** $p < 0.01$.

Table 3. Comparison of the seasonal and annual GPP derived from the tower estimates with those derived from the MODIS algorithms (MOD_NCEP GPP, MOD_Tower GPP, NCEP_GLASS GPP, and Tower_GLASS GPP).

Comparison	R^2	Mean (SD)	Bias	RMSE	RE
Seasonal		**(gC·m^{-2}·3-month^{-1})**	**(gC·m^{-2}·3-month^{-1})**	**(%)**	**(%)**
Spring (March–May)					
Flux_Tower *vs.* MOD_NCEP	0.64 **	322(265) *vs.* 283(229)	−39	50	56
Flux_Tower *vs.* MOD_Tower	0.62 **	322(265) *vs.* 200(200)	−122	63	55
Flux_Tower *vs.* NCEP_GLASS	0.56 **	322(265) *vs.* 362(265)	40	58	75
Flux_Tower *vs.* Tower_GLASS	0.65 **	322(265) *vs.* 242(211)	−80	54	44
Summer (June–August)					
Flux_Tower *vs.* MOD_NCEP	0.46 **	556(266) *vs.* 413(153)	−143	43	35
Flux_Tower *vs.* MOD_Tower	0.36 **	556(266) *vs.* 302(122)	−254	60	50
Flux_Tower *vs.* NCEP_GLASS	0.52 **	556(266) *vs.* 546(212)	−10	33	33
Flux_Tower *vs.* Tower_GLASS	0.43 **	556(266) *vs.* 395(162)	−161	46	41
Autumn (September–November)					
Flux_Tower *vs.* MOD_NCEP	0.80 **	337(238) *vs.* 337(243)	0	32	69
Flux_Tower *vs.* MOD_Tower	0.73 **	337(238) *vs.* 235(176)	−102	48	62
Flux_Tower *vs.* NCEP_GLASS	0.76 **	337(238) *vs.* 338(268)	1	38	57
Flux_Tower *vs.* Tower_GLASS	0.71 **	337(238) *vs.* 235(193)	−102	48	58
Winter (January, February and December)					
Flux_Tower *vs.* MOD_NCEP	0.92 **	116(137) *vs.* 137(197)	21	68	-
Flux_Tower *vs.* MOD_Tower	0.87 **	116(137) *vs.* 91(141)	−25	48	-
Flux_Tower *vs.* NCEP_GLASS	0.92 **	116(137) *vs.* 164(227)	48	98	-
Flux_Tower *vs.* Tower_GLASS	0.88 **	116(137) *vs.* 101(155)	−15	48	-

Table 3. *Cont.*

Comparison	R^2	Mean (SD)	Bias	RMSE	RE
Annual		**(gC· m^{-2}· year^{-1})**	**(gC· m^{-2}· year^{-1})**	**(%)**	**(%)**
Flux_Tower *vs.* MOD_NCEP	0.76 **	1331(806) *vs.* 1170(731)	−161	31	34
Flux_Tower *vs.* MOD_Tower	0.72 **	1331(806) *vs.* 827(559)	−504	50	44
Flux_Tower *vs.* NCEP_GLASS	0.68 **	1331(806) *vs.* 1410(913)	79	39	35
Flux_Tower *vs.* Tower_GLASS	0.69 **	1331(806) *vs.* 972(664)	−359	43	38

Significance levels: ** $p < 0.01$.

3.1.3. Annual GPP

The tower-based GPP measurements (Flux_Tower GPP) were compared with the results of the four algorithms (*i.e.*, MOD_NCEP GPP, MOD_Tower GPP, NCEP_GLASS GPP, and Tower_GLASS GPP) during 2003–2005. (Figure 8, Table 3). For all the sites, the annual average value of the Flux_Tower GPP was 1331 gC· m^{-2}· year^{-1}, and those of the four algorithms were 1170 gC· m^{-2}· year^{-1}, 827 gC· m^{-2}· year^{-1}, 1410 gC· m^{-2}· year^{-1} and 972 gC· m^{-2}· year^{-1}, respectively. The NCEP_GLASS GPP algorithm accurately estimated the measurements for CBS, QYZ and HB (Figure 8c) and therefore had the smallest bias (79 gC· m^{-2}· year^{-1}). However, for the MOD_Tower GPP and Tower_GLASS GPP algorithms, the Flux_Tower GPP for CBS, HB, QYZ, XSBN and YC were severely underestimated (Figure 8b,d), which led to large biases (−504 gC· m^{-2}· year^{-1} for MOD_Tower GPP and −359 gC· m^{-2}· year^{-1} for Tower_GLASS GPP). In terms of the estimating effectiveness, the MOD_NCEP GPP algorithm had the greatest performance because it yielded the largest R^2 (0.76) and smallest RMSE (31%) and RE (34%).

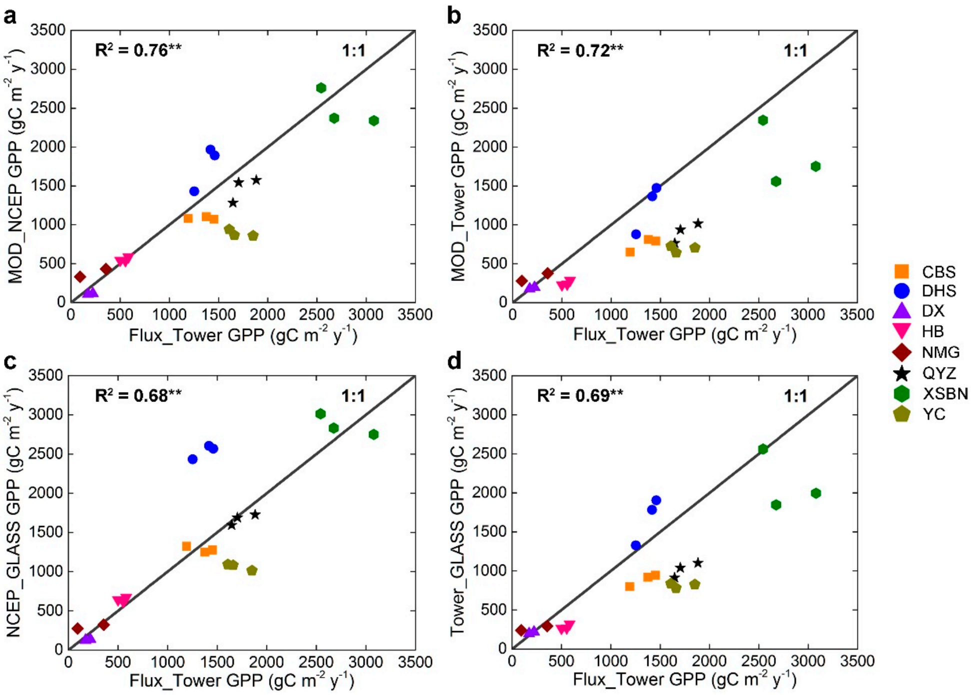

Figure 8. Comparisons of the annual Flux_Tower GPP with: (**a**) MOD_NCEP GPP; (**b**) MOD_Tower GPP; (**c**) NCEP_GLASS GPP; and (**d**) Tower_GLASS GPP. Significance levels: ** $p < 0.01$.

Based on the various biome types, the tower-based GPP measurements (Flux_Tower GPP) were compared with the results of the four algorithms (*i.e.*, MOD_NCEP GPP, MOD_Tower GPP, NCEP_GLASS GPP, and Tower_GLASS GPP) over several years (Table 4). In the case of MF, the Tower_GLASS GPP algorithm exhibited a significant correlation (R^2 = 0.97), though it seriously underestimated the Flux_Tower GPP (−454 gC· m^{-2}· year^{-1}). For ENF, the estimated results of the four algorithms were not statistically significant. The NCEP_GLASS GPP algorithm performed relatively well and had the smallest bias (−76 gC· m^{-2}· year^{-1}), RMSE (6%) and RE (4%). For EBF, the MOD_NCEP GPP algorithm was the most effective; it exhibited a significant correlation (R^2 = 0.58) and the smallest bias (55 gC· m^{-2}· year^{-1}), RMSE (22%) and RE (21%). For Crop, none of the algorithms provided effective estimates, with the exception of the NCEP_GLASS GPP algorithm, which also exhibited a significant correlation (R^2 = 0.98) and the smallest bias (−645 gC· m^{-2}· year^{-1}), RMSE (39%) and RE (37%). Regarding Grass, the NCEP_GLASS GPP algorithm outperformed the other algorithms due to its significant correlation (R^2 = 0.80) and smallest RMSE (29%) and RE (46%).

Table 4. Biome-based comparison of the annual GPP derived from the tower estimates with those derived from the MODIS algorithms (MOD_NCEP GPP, MOD_Tower GPP, NCEP_GLASS GPP, and Tower_GLASS GPP).

Comparison	R^2	Mean (SD) (gC· m^{-2}· year^{-1})	Bias (gC· m^{-2}· year^{-1})	RMSE (%)	RE (%)
Mixed Forest					
Flux_Tower *vs.* MOD_NCEP	-	1341(110) *vs.* 1085(14)	−256	21	19
Flux_Tower *vs.* MOD_Tower	0.71 *	1341(110) *vs.* 752(72)	−589	44	44
Flux_Tower *vs.* NCEP_GLASS	0.27	1341(110) *vs.* 1281(32)	−60	11	11
Flux_Tower *vs.* Tower_GLASS	0.97 *	1341(110) *vs.* 887(64)	−454	34	34
Evergreen Needleleaf Forest					
Flux_Tower *vs.* MOD_NCEP	0.14	1745(100) *vs.* 1467(131)	−278	17	16
Flux_Tower *vs.* MOD_Tower	0.55	1745(100) *vs.* 906(105)	−839	48	48
Flux_Tower *vs.* NCEP_GLASS	0.50	1745(100) *vs.* 1669(56)	−76	6	4
Flux_Tower *vs.* Tower_GLASS	0.58	1745(100) *vs.* 1019(78)	−726	42	42
Evergreen Broadleaf Forest					
Flux_Tower *vs.* MOD_NCEP	0.58 *	2072(715) *vs.* 2127(423)	55	22	21
Flux_Tower *vs.* MOD_Tower	0.34	2072(715) *vs.* 1562(441)	−510	35	21
Flux_Tower *vs.* NCEP_GLASS	0.52 *	2072(715) *vs.* 2700(190)	628	41	48
Flux_Tower *vs.* Tower_GLASS	0.18	2072(715) *vs.* 1903(363)	−169	29	21
Cropland					
Flux_Tower *vs.* MOD_NCEP	-	1707(105) *vs.* 888(38)	−819	49	48
Flux_Tower *vs.* MOD_Tower	-	1707(105) *vs.* 690(36)	−1017	60	59
Flux_Tower *vs.* NCEP_GLASS	0.98 *	1707(105) *vs.* 1062(35)	−645	39	37
Flux_Tower *vs.* Tower_GLASS	-	1707(105) *vs.* 814(25)	−893	53	52
Grassland					
Flux_Tower *vs.* MOD_NCEP	0.65 **	354(182) *vs.* 379(185)	25	30	53
Flux_Tower *vs.* MOD_Tower	-	354(182) *vs.* 255(61)	−99	58	55
Flux_Tower *vs.* NCEP_GLASS	0.80 **	354(182) *vs.* 399(223)	45	29	46
Flux_Tower *vs.* Tower_GLASS	0.52 *	354(182) *vs.* 258(39)	−96	51	48

Significance levels: * $p < 0.05$, ** $p < 0.01$.

3.2. Meteorology

In this paper, the MOD_NCEP GPP algorithm followed the standard MOD17A2 algorithm, which used the NCEP-DOE Reanalysis II meteorology data. However, the NCEP-DOE Reanalysis II meteorology data were replaced with the site meteorology data for use with the MOD_Tower GPP algorithm. Thus, the MOD_NCEP GPP and MOD_Tower GPP algorithms were compared to study the impacts of the meteorological data on the estimation results. An analysis of the seasonal and annual GPP estimates showed that the MOD_Tower GPP algorithm with the site meteorology data was inferior to the MOD_NCEP GPP algorithm (Table 3). However, in the case of the eight-day GPP estimates, the estimating effectiveness of the MOD_Tower GPP algorithm was better than that of the MOD_NCEP GPP algorithm, and the improvements were seen at most of the sites (Table 2).

The correlations between the daily NCEP-DOE Reanalysis II meteorology data and the daily site meteorology data were analyzed (Figure 9). The results demonstrated significant correlations between the two types of data in terms of T_{avg} (R^2 = 0.92) and T_{min} (R^2 = 0.90) (Figure 9a,b). This meant that the meteorological reanalysis datasets could be used to effectively estimate the on-site temperature variations. However, in the case of VPD_{avg}, the correlation between the NCEP-DOE Reanalysis II meteorology data and the site meteorology data was poor (R^2 = 0.31) (Figure 9c) because the meteorological reanalysis datasets failed to estimate the on-site moisture conditions. Regarding PAR, the NCEP-DOE Reanalysis II meteorology data commonly overestimated the site meteorology data (Figure 9d). The correlation (R^2 = 0.62) was stronger than that of VPD_{avg} but weaker than those of T_{avg} and T_{min}.

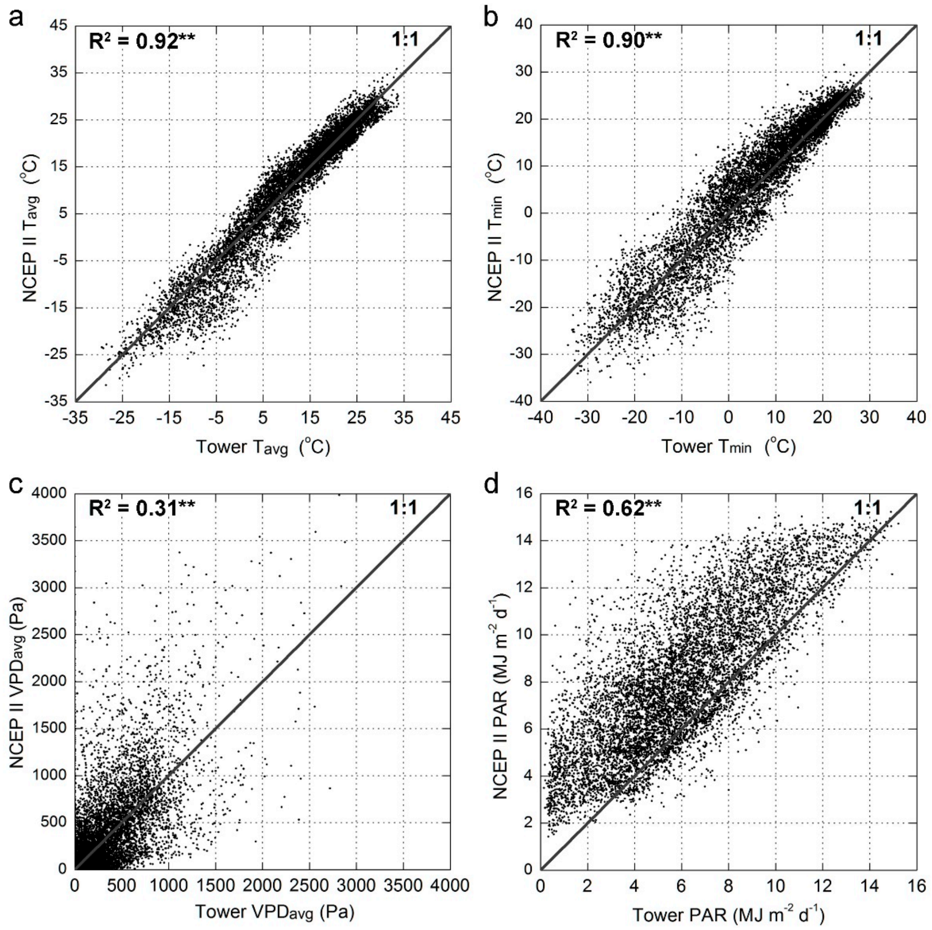

Figure 9. Scatterplots of the daily NCEP-DOE II meteorology against the daily tower meteorological data for: (**a**) T_{avg}; (**b**) T_{min}; (**c**) VPD_{avg}; and (**d**) PAR. Significance levels: ** $p < 0.01$.

3.3. LAI and FPAR

Unlike the MOD_NCEP GPP algorithm, the NCEP_GLASS GPP algorithm followed the MOD17A2 algorithm by substituting GLASS_FPAR (*i.e.*, the FPAR derived from GLASS LAI datasets) for MODIS_FPAR. Therefore, comparing the MOD_NCEP GPP and NCEP_GLASS GPP algorithms was helpful for understanding the influences of FPAR on the estimating effectiveness. Similar to the MOD_Tower GPP algorithm, the NCEP_GLASS GPP algorithm was outperformed by the MOD_NCEP GPP algorithm in terms of the annual GPP estimates (Table 3). However, regarding the seasonal estimates, the effectiveness of the NCEP_GLASS GPP algorithm for estimating the Flux_Tower GPP was better than that of the MOD_Tower GPP algorithm, which was vastly inferior to the MOD_NCEP GPP algorithm. In particular, no algorithm was more accurate than the NCEP_GLASS GPP algorithm for estimating the Flux_Tower GPP in the summer. In addition, the NCEP_GLASS GPP algorithm achieved substantial improvements over the MOD_NCEP GPP algorithm for the eight-day estimates (Figure 2a,c). It estimated the Flux_Tower GPP for CBS, QYZ and DHS far more effectively than the MOD_NCEP GPP algorithm (Table 2).

Comparisons were made between GLASS_LAI and MODIS_LAI as well as GLASS_FPAR and MODIS_FPAR (Figure 10 and Table 5). The results showed extremely significant correlations for the average values of LAI (R^2 = 0.93) and FPAR (R^2 = 0.91). MODIS_FPAR underestimated GLASS_FPAR in all of the eight sites except in NMG and DX. In particular, CBS, HB and DX exhibited the strongest correlations between MODIS_FPAR and GLASS_FPAR, and DHS, QYZ and XSBN exhibited relatively poor correlations (Figure 10b). From the perspective of the biomes, the correlations between MODIS_FPAR and GLASS_FPAR were strong for MF and poor for EBF.

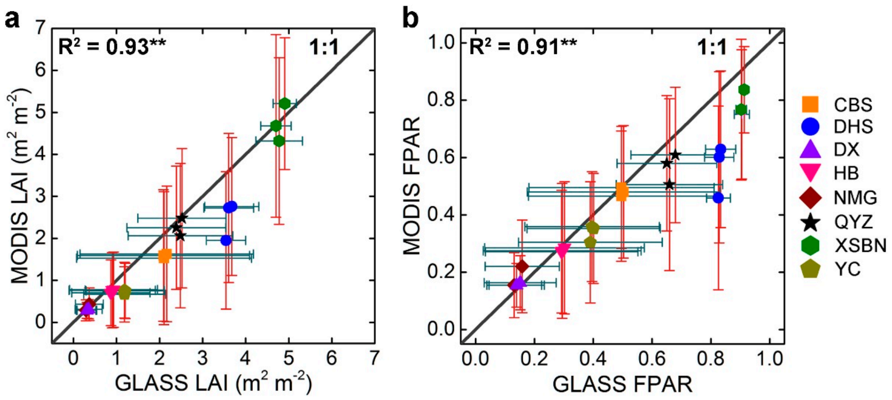

Figure 10. Comparison of the average (**a**) LAI and (**b**) FPAR from the MODIS datasets and the GLASS LAI products. Significance levels: ** $p < 0.01$.

Table 5. Comparison of the LAI and FPAR derived from the GLASS LAI datasets with those from the MODIS products for various biomes.

Site (Biome)	Comparison	Mean (SD)	Bias	RMSE (%)
CBS (**MF**)	GLASS_LAI *vs.* MODIS_LAI ($m^2 \cdot m^{-2}$) GLASS_FPAR *vs.* MODIS_FPAR	2.120(0.041) *vs.* 1.583(0.051) 0.498(0.004) *vs.* 0.480(0.015)	−0.537 −0.018	25 4
QYZ (**ENF**)	GLASS_LAI *vs.* MODIS_LAI ($m^2 \cdot m^{-2}$) GLASS_FPAR *vs.* MODIS_FPAR	2.464(0.055) *vs.* 2.267(0.170) 0.663(0.012) *vs.* 0.565(0.043)	−0.197 −0.098	10 16
DHS (EBF)	GLASS_LAI *vs.* MODIS_LAI ($m^2 \cdot m^{-2}$) GLASS_FPAR *vs.* MODIS_FPAR	3.609(0.055) *vs.* 2.478(0.373) 0.829(0.003) *vs.* 0.563(0.074)	−1.131 −0.266	33 33
XSBN (EBF)	GLASS_LAI *vs.* MODIS_LAI ($m^2 \cdot m^{-2}$) GLASS_FPAR *vs.* MODIS_FPAR	4.795(0.084) *vs.* 4.737(0.366) 0.907(0.004) *vs.* 0.785(0.037)	−0.058 −0.122	7 14
YC (**Crop**)	GLASS_LAI *vs.* MODIS_LAI ($m^2 \cdot m^{-2}$) GLASS_FPAR *vs.* MODIS_FPAR	1.192(0.007) *vs.* 0.728(0.044) 0.396(0.004) *vs.* 0.339(0.024)	−0.464 −0.057	39 15
HB (Grass)	GLASS_LAI *vs.* MODIS_LAI ($m^2 \cdot m^{-2}$) GLASS_FPAR *vs.* MODIS_FPAR	0.901(0.026) *vs.* 0.749(0.032) 0.296(0.004) *vs.* 0.277(0.006)	−0.152 −0.019	17 7
NMG (Grass)	GLASS_LAI *vs.* MODIS_LAI ($m^2 \cdot m^{-2}$) GLASS_FPAR *vs.* MODIS_FPAR	0.332(0.038) *vs.* 0.361(0.072) 0.145(0.014) *vs.* 0.188(0.033)	0.029 0.043	13 32
DX (Grass)	GLASS_LAI *vs.* MODIS_LAI ($m^2 \cdot m^{-2}$) GLASS_FPAR *vs.* MODIS_FPAR	0.333(0.020) *vs.* 0.299(0.014) 0.146(0.006) *vs.* 0.159(0.004)	−0.034 0.013	10 9
EBF	GLASS_LAI *vs.* MODIS_LAI ($m^2 \cdot m^{-2}$) GLASS_FPAR *vs.* MODIS_FPAR	4.202(0.597) *vs.* 3.607(1.189) 0.868(0.039) *vs.* 0.674(0.126)	−0.595 −0.194	21 25
Grass	GLASS_LAI *vs.* MODIS_LAI ($m^2 \cdot m^{-2}$) GLASS_FPAR *vs.* MODIS_FPAR	0.576(0.283) *vs.* 0.510(0.214) 0.210(0.075) *vs.* 0.218(0.056)	−0.066 0.008	18 14

3.4. Land Cover

The four algorithms used the MCD12Q1 Land Cover Classification Type 2 as their land cover classification scheme. The results of the land cover classification directly determine the value of the maximum light use efficiency (ε_{max}) and further influence the estimation results. Based on the user's guide for flux data provided by ChinaFLUX, we obtained the actual land cover type of each site. By comparing the MCD12Q1-based classification results with the actual land cover types at all eight sites, we found that MCD12Q1 correctly classified most of the sites (Figure 11). The only mistake was that MCD12Q1 misclassified the QYZ site to the MF category (the actual land cover was ENF).

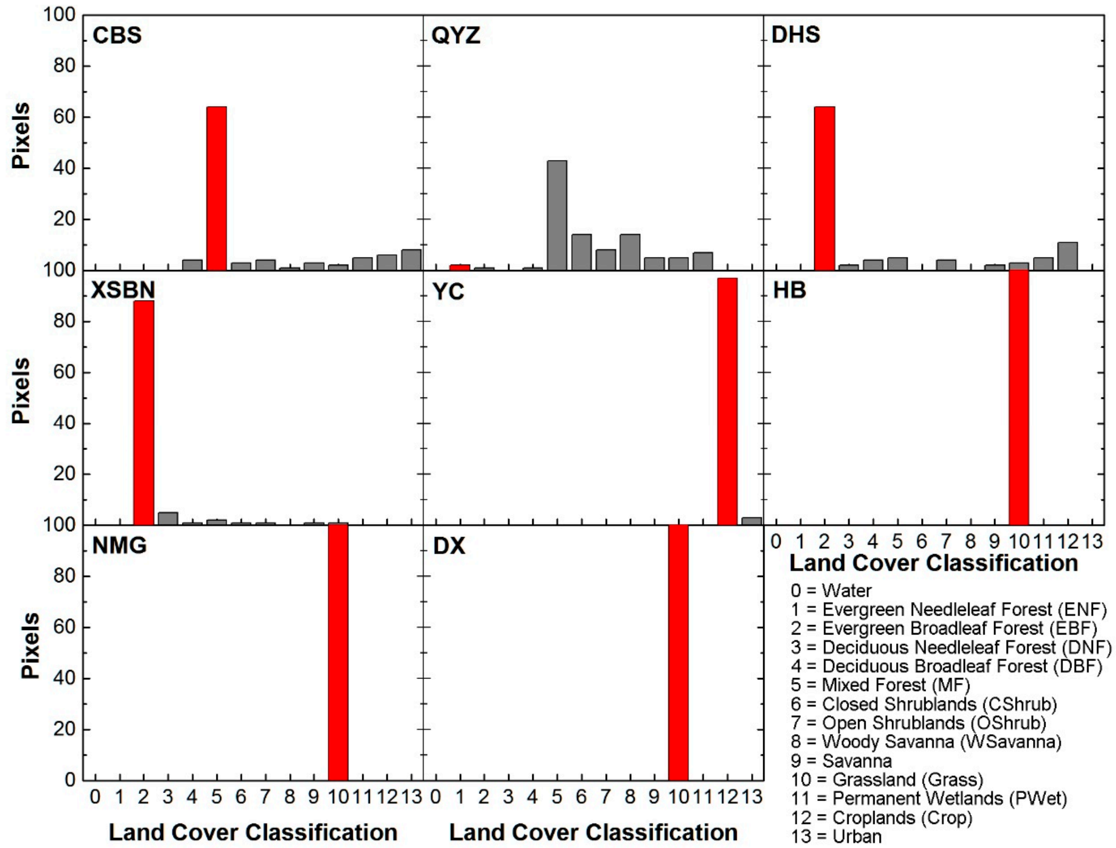

Figure 11. University of Maryland (UMD) land cover classification (MCD12Q1 Collection 5.1, Land Cover Classification Type 2) for the eight sites. The red columns indicate the actual land cover at each site.

3.5. Light Use Efficiency

For the MODIS GPP algorithm, the values of the maximum light use efficiency (ε_{max}) depend on the types of land cover. Each land cover type corresponds to a constant value of ε_{max}. Equations (1) and (3) in Section 2.1 were utilized to obtain the inferred ε_{max} for each land cover type, which were then compared with MOD17A2 ε_{max} directly (Figure 12 and Table 6). The results show that the inferred ε_{max} were higher than MOD17A2 ε_{max} by 60% for MF, 74% for ENF, 11% for EBF, 143% for Crop and 37% for Grass, respectively. However, in the case of a single site, the inferred ε_{max} were not invariably higher than MOD17A2 ε_{max}. For example, the inferred ε_{max} for DHS and NMG were less than the MOD17A2 ε_{max}.

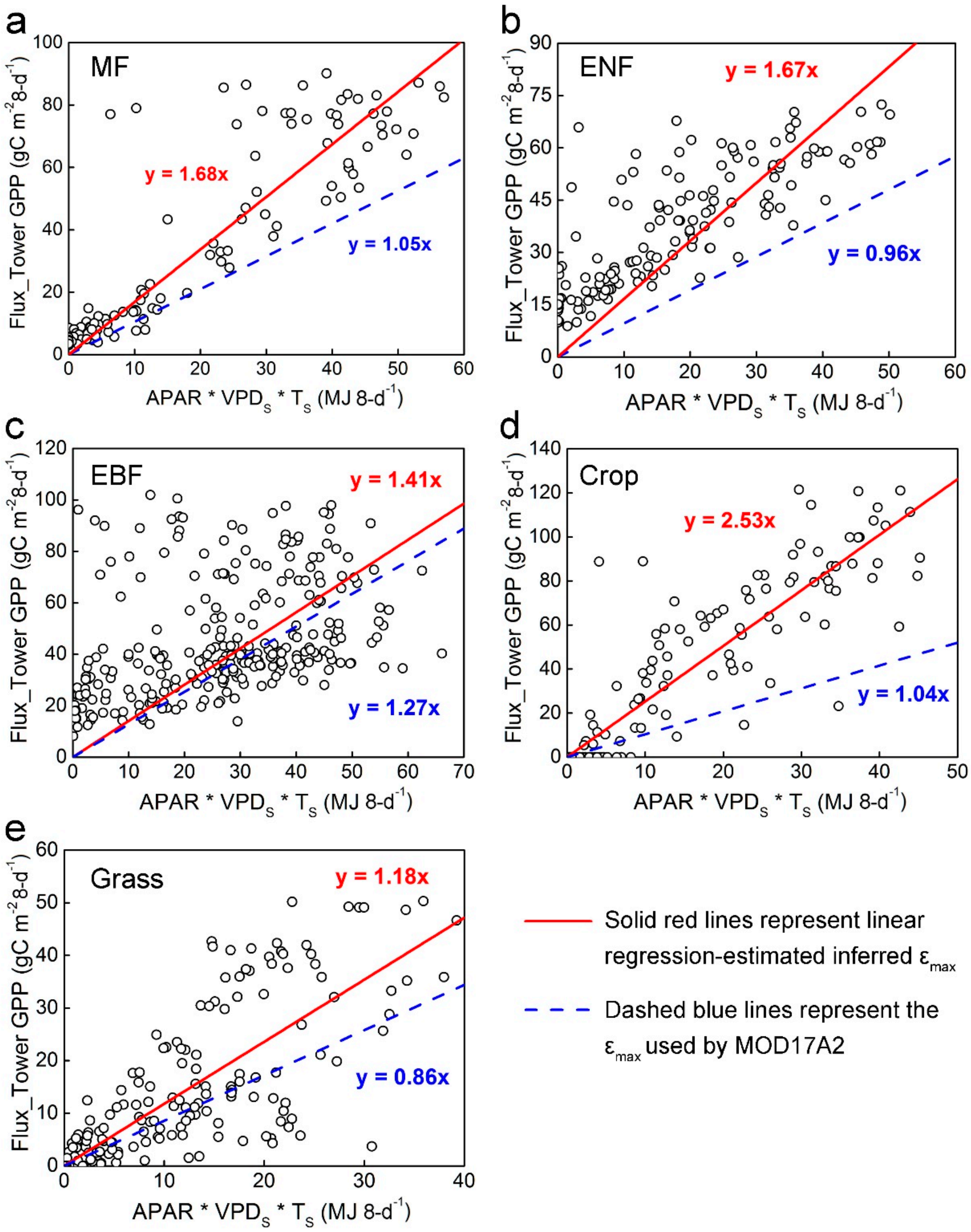

Figure 12. Eight-day tower estimated GPP (gC$\cdot$ m$^{-2}\cdot$ 8-day^{-1}) against the product of GLASS FPAR, tower PAR, VPD$_s$ and T$_s$ for: (**a**) Mixed forests; (**b**) Evergreen needleleaf forests; (**c**) Evergreen broadleaf forests; (**d**) Croplands; and (**e**) Grasslands. APAR (Absorbed Photosynthetic Active Radiation) = FPAR × PAR.

Table 6. Comparison of the inferred ε_{max} and MOD17A2 ε_{max} at the eight sites.

Site (Biome)	Inferred ε_{max}	MOD17A2 ε_{max}	Bias
CBS (MF)	1.68	1.05	−0.63
QYZ (ENF)	1.67	0.96	−0.71
DHS (EBF)	1.07	1.27	0.20
XSBN (EBF)	1.59	1.27	−0.32
YC (Crop)	2.53	1.04	−1.49
HB (Grass)	1.75	0.86	−0.89
NMG (Grass)	0.67	0.86	0.19
DX (Grass)	0.91	0.86	−0.05

4. Discussion

In this paper, GPP measurements from eight EC flux towers (Flux_Tower GPP) were used to verify four groups of GPP values calculated from the MODIS GPP algorithms (*i.e.*, MOD_NCEP GPP, MOD_Tower GPP, NCEP_GLASS GPP and Tower_GLASS GPP). The results show that the four groups of GPP values deviated from the tower-based GPP values to varying degrees. The extent of the deviations varied depending on the time interval, the site and the biome type used in the calculation. The deviations can be attributed to many potential factors. Clearly, the accuracy of each parameter input in the MODIS GPP formula will influence the accuracy of the GPP estimates. That is, the meteorology, LAI/FPAR, land cover and ε_{max} data are all error sources [48]. Furthermore, the accuracies of the tower-based GPP measurements and the reasonableness of the MODIS GPP algorithm itself should also be taken into account [49].

4.1. Impact of Meteorology on MODIS GPP

The PAR in the MODIS GPP algorithm together with T_{min} and VPD_{avg}, which influence LUE, are all meteorological factors. Thus, the meteorological inputs may be the largest sources of error in the GPP estimates [50]. The NCEP-DOE Reanalysis II meteorology dataset used in the C5.5 version of MOD17A2 product has a low resolution. Although a strict interpolation was used to make the resolution comparable to the MOD15A2 product, the errors caused by the original low resolution could not be eliminated completely. In addition, the interpolation process produces new uncertainties. From comparisons between the meteorological reanalysis data and the site meteorology data, it can be clearly observed that the NCEP-DOE Reanalysis II meteorology data are ineffective for estimating PAR, and the outcome is even worse for VPD (Figure 9c,d). In fact, the MODIS GPP algorithm does not directly take the soil moisture into account. However, soil moisture plays a key role in GPP estimation [51]. To compensate for this defect, the VPD was added to the algorithm as a proxy for the soil moisture; however, errors will be unavoidably introduced. In particular, the estimation error will increase when the deviations between the VPD estimates and measurements are large.

In this paper, we replaced the NCEP-DOE Reanalysis II meteorology data with the site meteorology data to recalculate the MODIS GPP formula and obtained new GPP values (*i.e.*, MOD_Tower GPP). Unexpectedly, the GPP estimates over eight days calculated using the site meteorology data did not result in obvious improvements in the accuracy of the GPP estimates (Figure 2a,b). On the contrary, the estimates of the seasonal and annual GPP calculated using the site meteorology data were not as accurate as those calculated using the meteorological reanalysis data (Table 3). This implies that improved meteorological inputs will not necessarily enhance the estimation effectiveness of the MODIS GPP algorithm, highlighting the need to analyze other sources of error.

4.2. Impact of LAI/FPAR on MODIS GPP

In addition to improving the quality of the meteorological inputs, we also introduced an improved LAI dataset (GLASS LAI) to evaluate the impacts of LAI/FPAR on the GPP estimates (*i.e.*, NCEP_GLASS GPP). The results show that after replacing MODIS FPAR with GLASS FPAR, substantial improvements were achieved in estimating the eight-day GPP values (Figure 2a,c). The effectiveness in estimating GPP during the summer was also improved (Figure 5a,c). For Cropland and Grassland, the GPP estimates became more accurate after FPAR was improved (Table 4). Based on the comparisons, it was found that the MODIS LAI/FPAR were generally less than the GLASS LAI/FPAR (Table 5). Indeed, the MOD17A2 GPP algorithm generally underestimated the tower-based GPP (Table 3). Therefore, the improved LAI/FPAR compensated for the underestimation caused by MODIS LAI/FPAR to some extent, which resulted in a higher effectiveness of the GPP estimation.

In this paper, we further estimated GPP by improving the quality of the meteorological inputs and the LAI/FPAR data jointly (*i.e.*, Tower_GLASS GPP). We simply replaced the NCEP-DOE Reanalysis II meteorology data with the site meteorology data and replaced MODIS FPAR with GLASS FPAR.

The results demonstrate that the replacements resulted in the greatest improvements in estimating the eight-day GPP values (Figure 2a,d). However, this type of replacement strategy was not very effective in estimating the seasonal and annual GPP (Table 3). This implies that the GPP estimation accuracy can be greatly improved by simultaneously enhancing the quality of the multiple inputs of the MODIS GPP algorithm. However, it does not mean that improvements can be achieved simply by substituting the input parameters because the overall performance gains are by no means the sum of the individual gains. In the future, we will thoroughly study how to use the synergies among the individual gains to increase GPP estimation accuracy.

4.3. Impact of Land Cover on MODIS GPP

The impact of land cover classification on GPP estimation is non-negligible. In this paper, the land cover at site QYZ was of type ENF, but it was misclassified to type MF by MCD12Q1 (Figure 11). This misclassification directly led to the misestimation of the FPAR by MOD15A2 and the misjudgment of ε_{max} by BPLUT and thus affected the MOD17A2 GPP estimate for site QYZ.

4.4. Impact of LUE on MODIS GPP

Regarding the MODIS GPP algorithm, ε_{max} represents the maximum light use efficiency of the vegetation in photosynthesis. The value of ε_{max} will vary with the type of biome. For a given biome type, ε_{max} is set to a constant by BPLUT. Encouragingly, BPLUT corrected and updated the value of ε_{max} several times. However, because of the immense diversity of earth surface environments and climate conditions, assigning a constant value of ε_{max} to the same biome type does not conform to the truth [52]. The improved ε_{max} that we inferred for the eight sites in this paper greatly differed from the MOD17A2 ε_{max} that was specified by BPLUT (Figure 12 and Table 6). Because the value of ε_{max} provides the foundation for the actual light use efficiency, the misestimation of ε_{max} will inherently decrease the accuracies of the GPP estimates.

4.5. Uncertainties, Errors, and Accuracies

Note that our evaluation of MODIS GPP is based on the assumption that the GPP values measured by the EC flux tower are the ground truth. However, many uncertainties exist in the tower-based GPP measurements [53]. The tower GPP data used in this paper were calculated as the difference between the net ecosystem exchange (NEE) and ecosystem respiration (R_{eco}). The precise estimation of R_{eco} is difficult and can lead to systematic and random errors in estimating GPP. Furthermore, uncertainties also arise due to scale mismatches between the tower flux footprints and MODIS pixels. In addition, the MODIS GPP algorithm itself is also a potential error source in GPP estimation. Recently, many studies have examined the structural errors of the MODIS GPP algorithm [54–56]. For example, Zhang *et al.* (2012) [57] compared the MODIS GPP product with estimates from a two-leaf process-based model. Their results showed that the MODIS GPP algorithm cannot properly treat the contribution of shaded/sunlit leaves to the calculation of the total GPP.

We should also notice that the number of observations in the regression analysis could affect our estimation results. The seasonal and annual GPP reduced a lot the number of observations in relation to the eight-day data. This could be one reason why the eight-day data gave, in general terms, more accurate estimations.

5. Conclusions

In this study, we methodically evaluated the eight-day, seasonal and annual MODIS GPP using EC flux measurements at eight sites in five various biome types across China from 2003 to 2005. The sensitivity of MOD17A2 algorithm to meteorological data and LAI/FPAR products were examined by introducing site meteorological measurements and improved GLASS LAI products. We also assessed the potential error contributions from land cover and ε_{max}. Each of these validation steps would help to isolate and identify sources of error. The main conclusions can be summarized as follow:

(1) The standard MOD17A2 product (*i.e.*, MOD_NCEP GPP) performed better at estimating the annual GPP (R^2 = 0.76) and agreed well with the tower GPP during the autumn (R^2 = 0.80) and winter (R^2 = 0.92). However, the effectiveness of the MOD_NCEP GPP algorithm for estimating GPP over eight days was poor (R^2 = 0.55) and even worse during the summer (R^2 = 0.46). In addition, the MOD_NCEP GPP algorithm was ineffective when estimating the annual GPP for mixed forests, evergreen needleleaf forests and cropland.

(2) Replacing the NCEP-DOE Reanalysis II meteorology data with the site meteorology data (*i.e.*, MOD_Tower GPP) only slightly improved the correlation with the tower GPP over eight days (R^2 = 0.56). However, substantial improvements in estimating the tower GPP over eight days (R^2 = 0.65) and during the summer (R^2 = 0.52) were achieved by substituting GLASS_FPAR for MODIS_FPAR (*i.e.*, NCEP_GLASS GPP). For cropland, the GPP estimates were more accurate after the FPAR data were improved. When the meteorology inputs and FPAR data were simultaneously replaced with improved data (*i.e.*, Tower_GLASS GPP), the effectiveness in estimating the tower GPP was improved significantly for mixed forests and evergreen needleleaf forests.

(3) There are four potential error sources related to the inputs of the MOD17A2 algorithm: meteorology, LAI/FPAR, land cover and ε_{max}. The NCEP-DOE Reanalysis II meteorology data failed in estimating the tower measured VPD (R^2 = 0.31), and MODIS_FPAR underestimated the improved FPAR data at most sites. Although MCD12Q1 succeeded in classifying most of the sites correctly, the values of MOD17A2 ε_{max} were much smaller than the optimized ε_{max} values for all five biome types discussed in this paper.

From above analysis, we suggest that the qualities of the meteorological data and LAI/FPAR products need to be improved and the BPLUT parameters should be adjusted to provide better GPP estimates using MOD17A2 for Chinese ecosystems. In future research, additional high-resolution LAI/FPAR and GPP products should be considered, such as MOD15A2H and MOD17A2H, which have been recently released.

Acknowledgments: We are grateful for the availability of the tower flux data from ChinaFLUX. We also acknowledge the China Meteorological Administration (CMA), which provided the observational meteorological datasets, and we would like to thank the Center for Global Change Data Processing and Analysis of Beijing Normal University for providing the GLASS LAI datasets.

Author Contributions: Hongji Zhu and Aiwen Lin designed the research; Hongji Zhu performed the experiments; Yu Xia analyzed the data; Hongji Zhu wrote the manuscript; and Lunche Wang and Ling Zou corrected and modified the manuscript.

Conflicts of Interest: The authors declare no conflict of interest.

References

1. Gebremichael, M.; Barros, A. Evaluation of MODIS Gross Primary Productivity (GPP) in tropical monsoon regions. *Remote Sens. Environ.* **2006**, *100*, 150–166. [CrossRef]
2. Beer, C.; Reichstein, M.; Tomelleri, E.; Ciais, P.; Jung, M.; Carvalhais, N.; Rodenbeck, C.; Arain, M.A.; Baldocchi, D.; Bonan, G.B.; *et al.* Terrestrial gross carbon dioxide uptake: Global distribution and covariation with climate. *Science* **2010**, *329*, 834–838. [CrossRef] [PubMed]
3. Kotchenova, S.Y.; Song, X.; Shabanov, N.V.; Potter, C.S.; Knyazikhin, Y.; Myneni, R.B. Lidar remote sensing for modeling gross primary production of deciduous forests. *Remote Sens. Environ.* **2004**, *92*, 158–172. [CrossRef]
4. Gitelson, A.A.; Viña, A.; Verma, S.B.; Rundquist, D.C.; Arkebauer, T.J.; Keydan, G.; Leavitt, B.; Ciganda, V.; Burba, G.G.; Suyker, A.E. Relationship between gross primary production and chlorophyll content in crops: Implications for the synoptic monitoring of vegetation productivity. *J. Geophys. Res.* **2006**, *111*. [CrossRef]
5. Yuan, W.; Liu, S.; Zhou, G.; Zhou, G.; Tieszen, L.L.; Baldocchi, D.; Bernhofer, C.; Gholz, H.; Goldstein, A.H.; Goulden, M.L.; *et al.* Deriving a light use efficiency model from eddy covariance flux data for predicting daily gross primary production across biomes. *Agric. For. Meteorol.* **2007**, *143*, 189–207. [CrossRef]

6. Sims, D.; Rahman, A.; Cordova, V.; Elmasri, B.; Baldocchi, D.; Bolstad, P.; Flanagan, L.; Goldstein, A.; Hollinger, D.; Misson, L. A new model of gross primary productivity for North American ecosystems based solely on the enhanced vegetation index and land surface temperature from MODIS. *Remote Sens. Environ.* **2008**, *112*, 1633–1646. [CrossRef]
7. Yang, Y.; Shang, S.; Guan, H.; Jiang, L. A novel algorithm to assess gross primary production for terrestrial ecosystems from MODIS imagery. *J. Geophys. Res.* **2013**, *118*, 590–605. [CrossRef]
8. Rahman, A.F. Potential of MODIS EVI and surface temperature for directly estimating per-pixel ecosystem C fluxes. *Geophys. Res. Lett.* **2005**, *32*. [CrossRef]
9. Wu, C.; Chen, J.M.; Huang, N. Predicting gross primary production from the enhanced vegetation index and photosynthetically active radiation: Evaluation and calibration. *Remote Sens. Environ.* **2011**, *115*, 3424–3435. [CrossRef]
10. Lin, A.; Zhu, H.; Wang, L.; Gong, W.; Zou, L. Characteristics of long-term climate change and the ecological responses in central China. *Earth Interact.* **2016**, *20*, 1–24. [CrossRef]
11. Zhao, M.; Heinsch, F.A.; Nemani, R.R.; Running, S.W. Improvements of the MODIS terrestrial gross and net primary production global data set. *Remote Sens. Environ.* **2005**, *95*, 164–176. [CrossRef]
12. Kanniah, K.D.; Beringer, J.; Hutley, L.B.; Tapper, N.J.; Zhu, X. Evaluation of Collections 4 and 5 of the MODIS Gross Primary Productivity product and algorithm improvement at a tropical savanna site in northern Australia. *Remote Sens. Environ.* **2009**, *113*, 1808–1822. [CrossRef]
13. Garbulsky, M.F.; Peñuelas, J.; Papale, D.; Ardö, J.; Goulden, M.L.; Kiely, G.; Richardson, A.D.; Rotenberg, E.; Veenendaal, E.M.; Filella, I. Patterns and controls of the variability of radiation use efficiency and primary productivity across terrestrial ecosystems. *Glob. Ecol. Biogeogr.* **2010**, *19*, 253–267. [CrossRef]
14. Heinsch, F.A.; Zhao, M.; Running, S.W.; Kimball, J.S.; Nemani, R.R.; Davis, K.J.; Bolstad, P.V.; Cook, B.D.; Desai, A.R.; Ricciuto, D.M.; *et al.* Evaluation of remote sensing based terrestrial productivity from MODIS using regional tower eddy flux network observations. *IEEE Tran. Geosci. Remote Sens.* **2006**, *7*, 1908–1925. [CrossRef]
15. Propastin, P.; Ibrom, A.; Knohl, A.; Erasmi, S. Effects of canopy photosynthesis saturation on the estimation of gross primary productivity from MODIS data in a tropical forest. *Remote Sens. Environ.* **2012**, *121*, 252–260. [CrossRef]
16. Coops, N.; Black, T.; Jassal, R.; Trofymow, J.; Morgenstern, K. Comparison of MODIS, eddy covariance determined and physiologically modelled gross primary production (GPP) in a Douglas-fir forest stand. *Remote Sens. Environ.* **2007**, *107*, 385–401. [CrossRef]
17. Groenendijk, M.; Dolman, A.J.; van der Molen, M.K.; Leuning, R.; Arneth, A.; Delpierre, N.; Gash, J.H.C.; Lindroth, A.; Richardson, A.D.; Verbeeck, H.; *et al.* Assessing parameter variability in a photosynthesis model within and between plant functional types using global Fluxnet eddy covariance data. *Agric. For. Meteorol.* **2011**, *151*, 22–38. [CrossRef]
18. Wu, C.; Munger, J.W.; Niu, Z.; Kuang, D. Comparison of multiple models for estimating gross primary production using MODIS and eddy covariance data in Harvard Forest. *Remote Sens. Environ.* **2010**, *114*, 2925–2939. [CrossRef]
19. Xiao, J.; Zhuang, Q.; Law, B.E.; Chen, J.; Baldocchi, D.D.; Cook, D.R.; Oren, R.; Richardson, A.D.; Wharton, S.; Ma, S. A continuous measure of gross primary production for the conterminous United States derived from MODIS and AmeriFlux data. *Remote Sens. Environ.* **2010**, *114*, 576–591. [CrossRef]
20. Turner, D.P.; Ritts, W.D.; Cohen, W.B.; Gower, S.T.; Zhao, M.; Running, S.W.; Wofsy, S.C.; Urbanski, S.; Dunn, A.L.; Munger, J.W. Scaling Gross Primary Production (GPP) over boreal and deciduous forest landscapes in support of MODIS GPP product validation. *Remote Sens. Environ.* **2003**, *88*, 256–270. [CrossRef]
21. Sjöström, M.; Zhao, M.; Archibald, S.; Arneth, A.; Cappelaere, B.; Falk, U.; de Grandcourt, A.; Hanan, N.; Kergoat, L.; Kutsch, W.; *et al.* Evaluation of MODIS gross primary productivity for Africa using eddy covariance data. *Remote Sens. Environ.* **2013**, *131*, 275–286. [CrossRef]
22. Wang, X.; Ma, M.; Li, X.; Song, Y.; Tan, J.; Huang, G.; Zhang, Z.; Zhao, T.; Feng, J.; Ma, Z.; *et al.* Validation of MODIS-GPP product at 10 flux sites in northern China. *Int. J. Remote Sens.* **2013**, *34*, 587–599. [CrossRef]
23. John, R.; Chen, J.; Noormets, A.; Xiao, X.; Xu, J.; Lu, N.; Chen, S. Modelling gross primary production in semi-arid Inner Mongolia using MODIS imagery and eddy covariance data. *Int. J. Remote Sens.* **2013**, *34*, 2829–2857. [CrossRef]

24. Zhang, Y.; Yu, Q.; Jiang, J.; Tang, Y. Calibration of Terra/MODIS gross primary production over an irrigated cropland on the North China Plain and an alpine meadow on the Tibetan Plateau. *Glob. Chang. Biol.* **2008**, *14*, 757–767. [CrossRef]
25. Liu, Z.; Shao, Q.; Liu, J. The performances of MODIS-GPP and -ET products in China and their sensitivity to input data (FPAR/LAI). *Remote Sens.* **2015**, *7*, 135–152. [CrossRef]
26. Guan, D.; Wu, J.; Zhao, X.; Han, S.; Yu, G.; Sun, X.; Jin, C. CO_2 fluxes over an old, temperate mixed forest in northeastern China. *Agric. For. Meteorol.* **2006**, *137*, 138–149. [CrossRef]
27. Wen, X.; Yu, G.; Sun, X.; Li, Q.; Liu, Y.; Zhang, L.; Ren, C.; Fu, Y.; Li, Z. Soil moisture effect on the temperature dependence of ecosystem respiration in a subtropical Pinus plantation of southeastern China. *Agric. For. Meteorol.* **2006**, *137*, 166–175. [CrossRef]
28. Zhang, L.; Yu, G.; Sun, X.; Wen, X.; Ren, C.; Fu, Y.; Li, Q.; Li, Z.; Liu, Y.; Guan, D.; *et al.* Seasonal variations of ecosystem apparent quantum yield (α) and maximum photosynthesis rate (P_{max}) of different forest ecosystems in China. *Agric. For. Meteorol.* **2006**, *137*, 176–187. [CrossRef]
29. Yu, G.; Wen, X.; Sun, X.; Tanner, B.D.; Lee, X.; Chen, J. Overview of ChinaFLUX and evaluation of its eddy covariance measurement. *Agric. For. Meteorol.* **2006**, *137*, 125–137. [CrossRef]
30. Sun, X.; Zhu, Z.; Wen, X.; Yuan, G.; Yu, G. The impact of averaging period on eddy fluxes observed at ChinaFLUX sites. *Agric. For. Meteorol.* **2006**, *137*, 188–193. [CrossRef]
31. Fu, Y.; Yu, G.; Sun, X.; Li, Y.; Wen, X.; Zhang, L.; Li, Z.; Zhao, L.; Hao, Y. Depression of net ecosystem CO_2 exchange in semi-arid Leymus chinensis steppe and alpine shrub. *Agric. For. Meteorol.* **2006**, *137*, 234–244. [CrossRef]
32. Monteith, J.L. Solar radiation and production in tropical ecosystems. *J. Appl. Ecol.* **1972**, *9*, 747–766. [CrossRef]
33. Running, S.W.; Thornton, P.E.; Nemani, R.R.; Glassy, J.M. Global terrestrial gross and net primary productivity from the Earth observing system. In *Methods in Ecosystem Science*; Sala, O., Jackson, R., Mooney, H., Eds.; Springer: New York, NY, USA, 2000; pp. 44–57.
34. Heinsch, F.A.; Reeves, M.; Votava, P.; Kang, S.; Milesi, C.; Zhao, M.; Glassy, J.; Jolly, W.M.; Loehman, R.; Bowker, C.F.; *et al. User's Guide: GPP and NPP (MOD17A2/A3) Products NASA MODIS Land Algorithm*; University of Montana: Missoula, MT, USA, 2003; p. 57.
35. Zhao, M.; Running, S.W. Drought-induced reduction in global terrestrial net primary production from 2000 through 2009. *Science* **2010**, *329*, 940–943. [CrossRef] [PubMed]
36. Level 1 and Atmosphere Archive and Distribution System (LAADS). Available online: https://ladsweb.nascom.nasa.gov/index.html (accessed on 3 May 2015).
37. Friedl, M.A.; Sulla-Menashe, D.; Tan, B.; Schneider, A.; Ramankutty, N.; Sibley, A.; Huang, X. MODIS collection 5 global land cover: Algorithm refinements and characterization of new datasets. *Remote Sens. Environ.* **2010**, *114*, 168–182. [CrossRef]
38. Earth System Research Laboratory. Available online: http://www.esrl.noaa.gov/psd/about/index.html (accessed on 11 May 2015).
39. China Meteorological Administration. Available online: http://cdc.nmic.cn/home.do (accessed on 7 June 2014).
40. Peng, Y.; Gitelson, A.A.; Sakamoto, T. Remote estimation of gross primary productivity in crops using MODIS 250 m data. *Remote Sens. Environ.* **2013**, *128*, 186–196. [CrossRef]
41. Xiao, Z.; Liang, S.; Wang, J.; Chen, P.; Yin, X.; Zhang, L.; Song, J. Use of general regression neural networks for generating the GLASS leaf area index product from time-series MODIS surface reflectance. *IEEE Trans. Geosci. Remote Sens.* **2014**, *52*, 209–223. [CrossRef]
42. Zhao, X.; Liang, S.; Liu, S.; Yuan, W.; Xiao, Z.; Liu, Q.; Cheng, J.; Zhang, X.; Tang, H.; Zhang, X.; *et al.* The Global Land Surface Satellite (GLASS) remote sensing data processing system and products. *Remote Sens.* **2013**, *5*, 2436–2450. [CrossRef]
43. Liang, S.; Zhao, X.; Liu, S.; Yuan, W.; Cheng, X.; Xiao, Z.; Zhang, X.; Liu, Q.; Cheng, J.; Tang, H.; *et al.* A long-term Global LAnd Surface Satellite (GLASS) data-set for environmental studies. *Int. J. Digit. Earth* **2013**, *6*, 5–33. [CrossRef]
44. Generation and Applications of Global Products of Essential Land Variables. Available online: http://glass-product.bnu.edu.cn (accessed on 21 July 2015).

45. Turner, D.P.; Ritts, W.D.; Cohen, W.B.; Gower, S.T.; Running, S.W.; Zhao, M.; Costa, M.H.; Kirschbaum, A.A.; Ham, J.M.; Saleska, S.R.; *et al.* Evaluation of MODIS NPP and GPP products across multiple biomes. *Remote Sens. Environ.* **2006**, *102*, 282–292. [CrossRef]
46. ChinaFLUX. Available online: http://www.chinaflux.org (accessed on 29 May 2015).
47. Yu, G.; Zhu, X.; Fu, Y.; He, H.; Wang, Q.; Wen, X.; Li, X.; Zhang, L.; Zhang, L.; Su, W.; *et al.* Spatial patterns and climate drivers of carbon fluxes in terrestrial ecosystems of China. *Glob. Chang. Biol.* **2013**, *19*, 798–810. [CrossRef] [PubMed]
48. He, M.; Zhou, Y.; Ju, W.; Chen, J.; Zhang, L.; Wang, S.; Saigusa, N.; Hirata, R.; Murayama, S.; Liu, Y. Evaluation and improvement of MODIS gross primary productivity in typical forest ecosystems of East Asia based on eddy covariance measurements. *J. For. Res.* **2013**, *18*, 31–40. [CrossRef]
49. Chen, J.; Zhang, H.; Liu, Z.; Che, M.; Chen, B. Evaluating parameter adjustment in the MODIS gross primary production algorithm based on eddy covariance tower measurements. *Remote Sens.* **2014**, *6*, 3321–3348. [CrossRef]
50. Zhao, M.; Running, S.W.; Nemani, R.R. Sensitivity of Moderate Resolution Imaging Spectroradiometer (MODIS) terrestrial primary production to the accuracy of meteorological reanalyses. *J. Geophys. Res.* **2006**, *111*. [CrossRef]
51. Mu, Q.; Zhao, M.; Heinsch, F.A.; Liu, M.; Tian, H.; Running, S.W. Evaluating water stress controls on primary production in biogeochemical and remote sensing based models. *J. Geophys. Res.* **2007**, *112*. [CrossRef]
52. Liu, Z.; Wang, L.; Wang, S. Comparison of different GPP models in China using MODIS image and ChinaFLUX data. *Remote Sens.* **2014**, *6*, 10215–10231. [CrossRef]
53. Moffat, A.M.; Papale, D.; Reichstein, M.; Hollinger, D.Y.; Richardson, A.D.; Barr, A.G.; Beckstein, C.; Braswell, B.H.; Churkina, G.; Desai, A.R.; *et al.* Comprehensive comparison of gap-filling techniques for eddy covariance net carbon fluxes. *Agric. For. Meteorol.* **2007**, *147*, 209–232. [CrossRef]
54. Nightingale, J.M.; Coops, N.C.; Waring, R.H.; Hargrove, W.W. Comparison of MODIS gross primary production estimates for forests across the U.S.A. with those generated by a simple process model, 3-PGS. *Remote Sens. Environ.* **2007**, *109*, 500–509. [CrossRef]
55. He, M.; Ju, W.; Zhou, Y.; Chen, J.; He, H.; Wang, S.; Wang, H.; Guan, D.; Yan, J.; Li, Y.; *et al.* Development of a two-leaf light use efficiency model for improving the calculation of terrestrial gross primary productivity. *Agric. For. Meteorol.* **2013**, *173*, 28–39. [CrossRef]
56. Hashimoto, H.; Wang, W.; Milesi, C.; Xiong, J.; Ganguly, S.; Zhu, Z.; Nemani, R. Structural uncertainty in model-simulated trends of global gross primary production. *Remote Sens.* **2013**, *5*, 1258–1273. [CrossRef]
57. Zhang, F.; Chen, J.M.; Chen, J.; Gough, C.M.; Martin, T.A.; Dragoni, D. Evaluating spatial and temporal patterns of MODIS GPP over the conterminous U.S. against flux measurements and a process model. *Remote Sens. Environ.* **2012**, *124*, 717–729. [CrossRef]